DEPARTMENT OF PHYSICS, UNIVERSITY OF JYVÄSKYLÄ
RESEARCH REPORT No. 17/1981

BETA-DELAYED PARTICLE EMISSION IN $T_z = -1$, $A = 4n$ $(5 \leq n \leq 10)$ NUCLEI

BY
JORMA HONKANEN

Academic dissertation
for the Degree of
Doctor of Philosophy

Jyväskylä, Finland
October 1981

URN:ISBN:978-951-39-9479-2
ISBN 978-951-39-9479-2 (PDF)
ISSN 0075-465X

Jyväskylän yliopisto, 2023

ISBN 951-678-590-5
ISSN 0075-465-X

DEPARTMENT OF PHYSICS, UNIVERSITY OF JYVÄSKYLÄ
RESEARCH REPORT No. 17/1981

BETA-DELAYED PARTICLE EMISSION IN $T_z = -1$, $A = 4n$ $(5 \leq n \leq 10)$ NUCLEI

BY
JORMA HONKANEN

Academic dissertation
for the Degree of
Doctor of Philosophy

To be presented, by permission of the
Faculty of Mathematics and Natural Sciences
of the University of Jyväskylä,
for public examination in Auditorium S-212 of the
University on October 17, 1981, at 12 o'clock noon.

Jyväskylä, Finland
October 1981

Preface

This work has been carried out during the years 1977 - 1981 at the Department of Physics, University of Jyväskylä. I wish to express my thanks to this institute for the excellent working conditions and to the many people, who have helped me throughout these years.

I am particularly indebted to Professor K. Eskola, for guiding me in the area of experimental nuclear physics. His continuous interest and encouragement during the course of this work have been of great value. I am also grateful to Professor K. Valli and Dr. J. Äystö for their support and suggestions. To my coworkers Dr. M. Kortelahti, Mr. A. Hautojärvi, Phil. Lic. and Mr. K. Vierinen, Phil. Lic., I am greatly indebted for their help. I am also indebted to Dr. Pirkko Eskola, who tailored the Coulomb barrier penetrability program to suit specifically for delayed particle emission.

I would like to thank the staffs of the cyclotron, of the computer, of the target laboratory and of the machine shop for their efficient co-operation. I am obliged to Miss Tuula Tuominen, who carefully typed this thesis, and to Mr. T. Näränen, who skillfully finished the drawings.

I want to especially thank my wife, Ulla, for her support during my work and for her accommodation to the insistent demands of experimental research and thesis writing.

This work has been financially supported by the Magnus Ehrnrooth Foundation and the Emil Aaltonen Foundation.

Jyväskylä, September 1981

Jorma Honkanen

BETA-DELAYED PARTICLE EMISSION IN $T_z = -1$, $A = 4n$ $(5 \leq n \leq 10)$ NUCLEI

Abstract

Studies of beta-delayed particle emission among the $T_z = -1$, $A = 4n$ $(5 \leq n \leq 10)$ series have been undertaken. These short-lived nuclides were produced via (p,n) reactions using 20 MeV protons. Helium-jet technique coupled to a fast tape-transport system was used for source preparation. High resolution and low background were achieved in particle spectra measured with Si(Au) surface-barrier detectors.

Both delayed proton and α-particle emission are energetically allowed in the studied nuclides. However, in the decay of ^{20}Na and ^{24}Al only delayed α-particle emission was observed, while the heavier nuclides ^{28}P, ^{32}Cl, ^{36}K and ^{40}Sc were found to be precursors of both delayed protons and α particles. Owing to the high particle separation energies in the emitter total particle branchings are small ranging from $4.4 \cdot 10^{-3}$ to $1.3 \cdot 10^{-5}$ for protons and from 0.20 to $9 \cdot 10^{-6}$ for α particles.

Absolute intensities of individual proton or alpha-particle transitions were measured and corresponding log ft values or their upper limits were determined for the preceding β^+ transitions. The observed β-decay rates were compared with those predicted by recent large-basis shell-model calculations. Spin, parity and isospin values were assigned to a large number of unbound levels on the basis of the selection rules governing β-decay and particle emission. Detailed comparisons of data derived from delayed particle and resonance reaction studies were made.

Contents

1. INTRODUCTION

An active search for and study of β-delayed particle emitters has resulted in the discovery of a large number of precursor nuclei and in increasing understanding of their nuclear properties[1,2]. A general trend in this research has been to probe nuclides more and more remote from the β-stability line[3,4]. However, in light nuclei β-delayed particle precursors are either known or predicted to exist also close to the line of β stability. Nuclei in the A = 4n mass series and with $T_z = -1$ form such a group. Those studied in this work are shown in fig. 1. All of them have Q_{EC} values well in excess of proton and α-particle binding energies in their daughter nuclei and have half-lives in the range of 0.1 to 2.1 s.

In previous studies delayed α particles have been observed in the decay of ^{20}Na[5], ^{24}Al[6,7], ^{24m}Al[7] and ^{32}Cl[6] and delayed protons in the decay of ^{32}Cl[6] and ^{40}Sc[8,9]. No delayed particles have been associated with the decay of ^{28}P and no delayed α particles with the decay of ^{40}Sc. While this work was in progress delayed particle emission of ^{36}K was reported[10]. The absolute particle-branching ratios have been measured only in the decay of ^{20}Na and ^{24}Al. In the present work simultaneous measurement of particle and γ-ray spectra allowed the determination of particle branching ratios for all nuclei in the $T_z = -1$ series. High resolution in charged-particle detection was achieved by using helium-jet technique to produce thin sources and by using single high-resolution surface-barrier detectors.

The β-delayed particle emission has been found to be an efficient method to obtain information about highly excited levels. Measurements of the particle energies and intensities permit the determination of excitation energies of states as well as the β-decay transition rates to these states. It is often possible to establish spin, parity and isospin for unbound levels

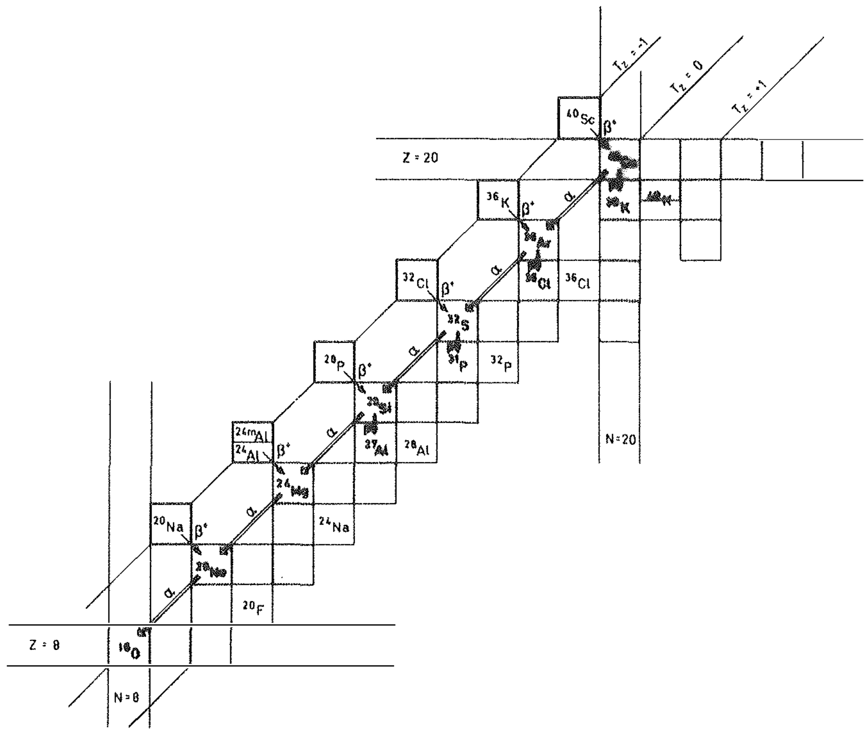

Fig. 1. A part of the chart of nuclides. The $T_z = -1$ nuclei studied in this work are shown by heavy solid frame. Their observed β^+-delayed α-particle and proton emissions are indicated by arrows. The mirror nuclei corresponding to $T_z = +1$ are also shown. Stable nuclei are shaded.

by applying the selection rules of β-decay and particle emission. Because proton, α-particle and γ-ray emissions are all energetically possible in the nuclei under study, these decay modes and their mutual competition can be studied. In some cases partial width ratios Γ_α/Γ_p can be directly obtained from the delayed particle spectrum. By combining them with corresponding resonance reaction data the partial widths can be deduced for several levels. Although the sensitivity of γ-ray detection is rarely sufficient to direct observation of γ branchings from unbound states, resonance yield measurements can give information on γ widths. Recent shell-model calculations[11)] provide both excitation energies and log ft values for many nuclei in the sd shell. The experimental measurements of log ft values for these transitions are a sensitive test of these calculations.

Some of the results of this thesis have previously been published in the following papers or reports:

1. J. Honkanen, M. Kortelahti, J. Äystö, K. Eskola and A. Hautojärvi, Physica Scripta 19 (1979) 239
2. J. Honkanen, M. Kortelahti, K. Valli, K. Eskola, A. Hautojärvi and K. Vierinen, Nucl. Phys. A330 (1979) 429
3. K. Eskola, M. Riihonen, K. Vierinen, J. Honkanen, M. Kortelahti and K. Valli, Nucl. Phys. A341 (1980) 365
4. J. Honkanen, M. Kortelahti, K. Valli, J. Äystö, K. Eskola, A. Hautojärvi and K. Vierinen, JYFL Annual Report 1978, 3.3., to be published

2. THEORY

2.1. Beta-delayed particle emission

The beta-delayed particle emission of a nuclide consists of two successive processes. First the nucleus β decays to an unbound state of the emitter, then the excitation is released by the emission of a particle. The lifetime of the unbound level is generally very short, $\lesssim 10^{-15}$ s ($\Gamma_\nu \gtrsim 1$ eV), and thus the delayed particles possess the same half-life as the precursor. In light nuclei the level densities are low and one usually observes well resolved peaks in delayed particle spectra. In consequence of this detailed information can be obtained about individual levels and preceding β transitions. For heavier nuclides individual transitions cannot generally be resolved and the delayed particle spectrum reflects average properties of the decay.

A decay scheme of a typical delayed particle precursor is shown in fig. 2. A minimum requirement for β-delayed particle emission is that the β-decay energy of the precursor exceeds the particle separation energy of the emitter. This condition is not sufficient to ensure that the particle-decay branch will be strong enough to be observed. For levels which are unbound by only a few hundred keV, the penetrability through Coulomb and centrifugal barriers may be so low that γ decay can compete favourably with particle emission. The probability that a level will decay through either channel is given in terms of partial widths. The γ width is nearly constant while the particle widths increase rapidly as a function of excitation energy. At a certain energy the particle and γ widths become comparable. This energy may be taken as an effective threshold for particle emission. Although the probability for particle emission increases with the excitation energy of the emitter, the rate at which states are populated by β decay decreases. The total intensity of particle emission is governed by the interplay of these two opposite factors. This results in a bell-shaped structure of the particle spectrum, which is clearly seen in the decay of heavier precursors.

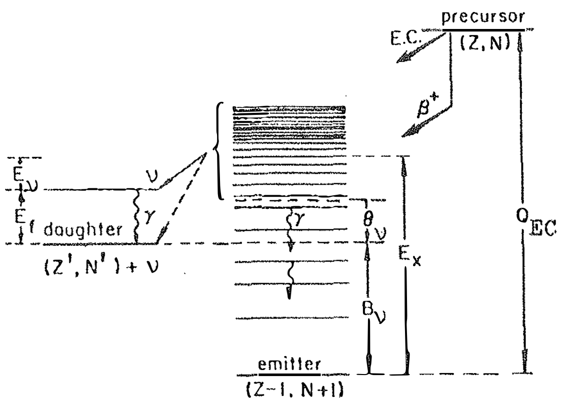

Fig. 2. Typical decay scheme of a delayed particle precursor illustrating some symbols and terms used in the text.

The particle branching ratio, or the intensity I_ν^{if} of a particle transition from a state i in the emitter to state f in the daughter, is given by[2)]

$$I_\nu^{if} = \frac{\Gamma_\nu^{if}}{\Gamma_i} I_\beta^i \, . \qquad (2.1)$$

Here Γ_ν^{if} is the partial width for the emission of a particle of type ν and Γ_i is the total width of the state i. The intensity I_β^i of the β transition to the state i in the emitter is given per disintegration of the precursor. The intensity I_β^i can be deduced from a measured branching ratio I_ν^{if}, only if both Γ_ν^{if} and Γ_i are known. However, since $I_\nu^{if} \leq I_\beta^i$, I_ν^{if} can be used to calculate an upper limit for the log ft value that characterizes the β transition to the state i.

2.2. Allowed beta decay

Using the notations of Raman et al.[12] the allowed β-decay strength is related to nuclear matrix elements by the expression

$$(1 + \delta_R)t = \frac{K/G'_V{}^2}{f_V\langle 1\rangle^2(1 - \delta_c) + f_A R_e^2\langle\sigma\tau\rangle^2} \quad , \tag{2.2}$$

where t is the partial half-life, δ_R and δ_c are the radiative and charge dependent mixing corrections, $\langle 1\rangle$ is the Fermi and $\langle\sigma\tau\rangle$ the Gamow-Teller matrix element, $K = 1.2306 \cdot 10^{-94}$ erg^2 cm^6 s, $G'_V = 1.4128 \cdot 10^{-49}$ erg cm^3 is the effective vector coupling constant and $R_e = G_{Ae}/G'_V = 1.237 \pm 0.008$ is the ratio of axial-vector and vector coupling constants. There is a small difference in the statistical rate function f between vector and axial-vector transitions as pointed out by Raman et al. This difference is typically only one or two per cent and thus the approximation $f_V = f_A = f$ is generally used. The β-decay strength is often presented in terms of reduced transition probabilities[13]. In consistency with eq. (2.2) and with $f_V = f_A = f$ the following expression for an allowed β transition is obtained

$$(1 + \delta_R)ft = \frac{6165 \text{ s}}{B'(F)\ (1 - \delta_c) + R_e^2 \cdot B'(GT)} \quad , \tag{2.3}$$

where B'(F) and B'(GT) are the reduced Fermi and GT transition probabilities B(F) and B(GT) in units of $g_V^2/4\pi$ and $g_A^2/4\pi$, respectively. For a pure GT transition the reduced transition probability is thus given by

$$B'(GT) = \frac{4030}{(1 + \delta_R)ft} \quad . \tag{2.4}$$

The Fermi and GT matrix elements between initial and final state wave functions are given as [12)]

$$\langle 1 \rangle^2 = \langle \psi_f \mid \sum_n \tau_\pm(n) \mid \psi_i \rangle = \langle \psi_f \mid T_\pm \mid \psi_i \rangle \tag{2.5}$$

$$\langle \sigma\tau \rangle^2 = \langle \psi_f \mid \sum_n \sigma(n)\, \tau_\pm(n) \mid \psi_i \rangle \tag{2.6}$$

where $\tau_\pm$ is the isospin raising (+) or lowering (-) operator for the n th nucleon and $\sigma(n)$ is the Pauli spin operator. Operator τ_+ converts a proton to a neutron (β^+ decay) and τ_- a neutron to a proton (β^- decay). The sum of the $\tau_\pm(n)$ operator over all n nucleons is defined as the total isospin operator $T_\pm$. The isospin operator raises or lowers the isospin projection T_z by one unit and thus analogous to the angular momentum raising or lowering operator

$$T_\pm \mid (J^\pi, T, T_z) \rangle = \left[(T \mp T_z)(T \pm T_z + 1) \right]^{1/2} \mid (J^\pi, T, T_z \pm 1) \rangle \, . \tag{2.7}$$

The isospin operator connects states that differ only in isospin projection and from this it follows that the selection rules for allowed Fermi transitions are $\Delta J = 0$, $\Delta\pi = 0$ and $\Delta T = 0$. In the case of pure isospin states $\langle 1 \rangle$

may be evaluated from eqs. (2.5) and (2.7) as

$$\langle 1 \rangle^2 = T(T+1) - T_{zi}T_{zf} \ . \qquad (2.8)$$

A pure Fermi transition from a T = 1, $T_z = -1$ initial state to a T = 1, $T_z = 0$ final state would then have $\langle 1 \rangle^2 = 2$ and correspondingly log ft = 3.49.

Evaluation of the GT matrix element is dependent upon the explicit details of the initial and final state wave functions. By applying the Wigner-Eckart theorem to the expression (2.6) the GT matrix element can be expressed by[14)]

$$\langle \sigma\tau \rangle^2 = \frac{\langle T_i T_{zi} \; 1 \pm 1 \mid T_f T_{zf} \rangle^2}{2(2J_i+1)(2T_f+1)} \langle J_f T_f \; ||| \sum_{n=1}^{A} \sigma(n)\,\tau(n) \; ||| \; J_i T_i \rangle^2 \ , \qquad (2.9)$$

where the first factor in brackets is a Clebsch-Gordan coefficient and the second one is a reduced matrix element. From the Clebsch-Gordan coefficients in this expression and conservation of parity one obtains the selection rules $\Delta J = 0,1$; $J_i = 0 \not\to J_f = 0$; $\Delta T = 0,1$; $\Delta\pi = 0$ for GT transitions. The GT matrix elements are calculable from equation (2.9) for different shell-model orbits by using two-particle interactions. Unfortunately, due to configuration mixing, most nuclear states cannot be accurately described by only one shell-model configuration. Thus the shell-model calculations, which allow configuration mixing between a large variety of different configurations, are in many cases necessary. Such calculations have been recently presented for sd-shell nuclei in the compilation of Brown and Wildenthal[11)]. At most, 6957 basis states are required to describe a state in the complete sd-shell base[15)].

The radiative correction in eq. (2.2) arises from the interaction of the decaying nucleon and the emitted charged lepton with the external electromagnetic field. These corrections are considered in two parts, the inner correction which is nuclide independent and the outer correction which depends on Z and the β-decay energy W_0. The former can effectively be considered as a renormalization of the β-decay coupling constant by $G'_V = G_V\,(1 + \Delta_R)$ [12]. The outer correction δ_R must be evaluated for each case. However, for Z < 20 it is in general below 2 %.

Mixing of states with different isospin arises from charge-dependent interactions. This causes the radial overlap integral of the parent and daughter nucleus to be less than unity. Isospin mixing has been considered[16] to arise from charge-dependent configuration mixing of states and differences in the neutron and proton wave functions. This mixing has been systematically studied[16,17,18] in pure $0^+ \rightarrow 0^+$ Fermi transitions. In these cases the isospin impurity correction δ_c has been deduced to be less than 1 %. However, the density of 0^+ levels in these nuclides is low and no notable configuration mixing is expected.

The statistical rate function is given in units of $m_e c^2$ by[12]

$$f = \int_1^{W_0} pW\,(W_0 - W)^2\,F(Z,W)\,C(W)\,dW\ , \qquad (2.10)$$

where W and p are the electron energy and momentum, W_0 is the maximum β energy, F(Z,W) is the Fermi function and C(W) is the shape correction factor. Gove and Martin have tabulated[19] the values of log f for allowed and first forbidden β transitions as a function of W_0 and Z. For allowed transitions they have used C(W) = 1. In the Fermi function they have taken into account the corrections due to nuclear charge distribution and the screening of atomic electrons. In the β^+ decay electron capture always competes with the β decay. This has been taken into account in the experimental log ft values by taking the statistical rate function to be $f = f_{\beta^+} + f_{EC}$.

Beta transitions can be classified into certain groups on the basis of the comparative half-life. According to a survey of Raman and Gove[20] all β transitions with log ft $\leq$ 5.9 are of the allowed type in elements lighter than mercury.

2.3. Isobaric analog states

The concept of the isobaric analog states arises from the charge independence of the nuclear force. This is supported by the observation that the energy spectra and β-decay transition rates of mirror nuclei are very much alike. Because the wave functions of analog states are identical, they have closely similar properties such as spectroscopic factors and electromagnetic transition rates. The isospin quantum number T is associated with these isobaric analog states. In light nuclei the isospin for the ground state is generally $T = |T_z| = |1/2\,(N - Z)|$. The binding energies of the analog states are identical once they are corrected for Coulomb energy and the mass difference between neutron and proton. A classical expression for the Coulomb energy is a sphere of radius R having constant charge density and total charge Z

$$E_C = \frac{3}{5}\,\frac{Z^2e^2}{R}\,. \tag{2.11}$$

A more accurate expression for the Coulomb displacement energy is obtained from a semiempirical formula[21]

$$\Delta E_C = 1.444\,\frac{\overline{Z}}{A^{1/3}} - 1.13\ \text{MeV}, \tag{2.12}$$

where A is the mass number and $\bar{Z}$ is the average charge. In light T = 1 multiplets the ground state analogs are known and the Coulomb displacement energies can be determined from the measured binding energies. In this work the experimental Coulomb displacement energy was used to assign the other analog states in a certain multiplet.

The energy scale in the decay of $T_z = -1$, $A = 4n$ nuclides referred to the ground state of the emitter is shown in fig. 3. The β-decay Q value (Q_{EC}) of the precursor, the excitation energy (E_A) and the proton and α-particle binding energies (B_p and B_α) in the emitter have been displayed. It can be seen in this figure that the energy window for α emission is much wider than for proton emission. In addition, α-particle emission is energetically possible from the analog states of ^{20}Na, ^{24}Al, ^{32}Cl and ^{40}Sc. However, taking into account the inhibiting influence of the Coulomb barrier, the α emission is expected to be observable only from the analog state in ^{20}Ne. Because the α particle has isospin zero, α transitions from T = 1 states in the emitter to the T = 0 ground state of the daughter nucleus are isospin forbidden. However, mixing of T = 0 and T = 1 states can occur so that α emission can take place via the T = 0 admixtures.

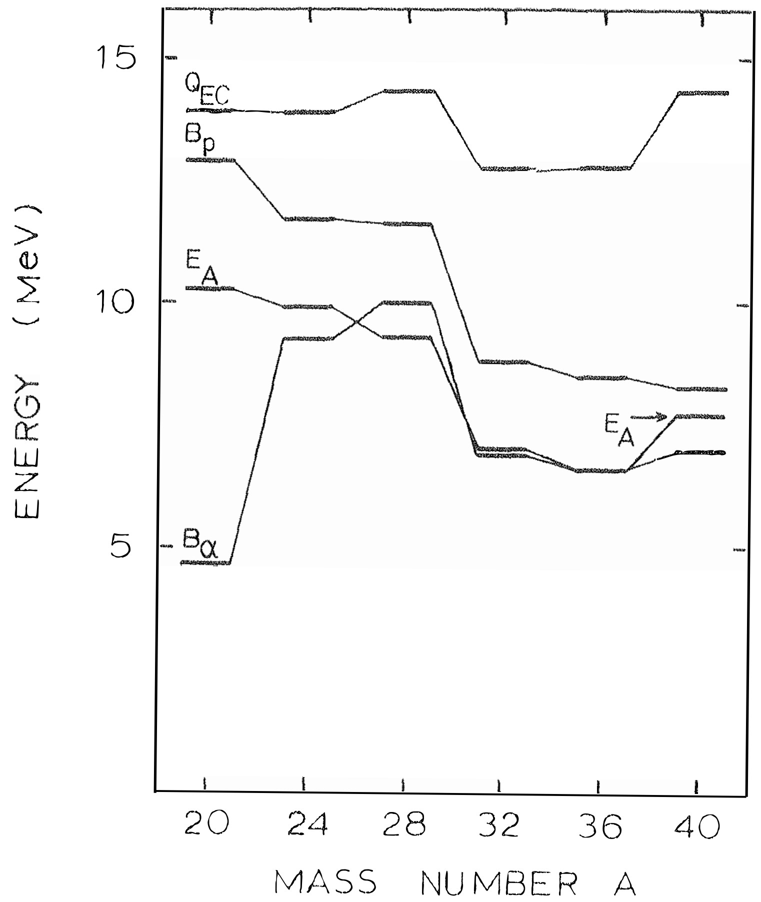

Fig. 3. The β-decay energies (Q_{EC}), the excitation energies of the T = 1 analog states (E_A) and the proton and α-particle separation energies (B_p and B_α) for particle emitters populated by the β decay of T_z = −1 precursors. All energies are relative to the emitter ground state.

2.4. Particle emission from unbound states

The particle decay of an unbound state depends on the degree of overlap between the initial and final state wave functions and on external kinematic effects of penetration through Coulomb and centrifugal barriers. These factors can be written out separately and the partial width for a given exit channel is given[1] by the expression

$$\Gamma = 2P_{\ell}\,\gamma^2 \ , \tag{2.13}$$

where P_ℓ is the penetrability through the Coulomb and angular momentum barriers and γ^2 is the reduced width. The internal nuclear structure effects are contained in γ^2. The angular momentum ℓ carried out by the emitted particle ν is related to the initial and final state spin and parity by

$$\begin{aligned} &|J_i - J_f| \pm s_\nu \leq \ell \leq J_i + J_f \pm s_\nu \\ &\Delta\pi = (-1)^{\ell} \ , \end{aligned} \tag{2.14}$$

where s_ν is the intrinsic spin of the emitted particle.

The penetrabilities are usually calculated employing the well-known regular and irregular Coulomb wave functions, F_ℓ and G_ℓ, respectively. The wave functions are the solutions to the Schrödinger equation using a Coulomb potential. The penetrability is then given by

$$P_\ell = \frac{kR}{F_\ell^{\,2} + G_\ell^{\,2}} \ , \tag{2.15}$$

where R is the nuclear radius and k is the wave number which is given by

$$k = \frac{(2\mu E)^{1/2}}{\hbar} = 0.2187\ (\mu E)^{1/2}\ \mathrm{fm}^{-1}\ , \tag{2.16}$$

where μ is the reduced mass in amu and E is the centre of mass energy in MeV. The Coulomb wave functions are evaluated at the nuclear radius

$$R = R_o\ (A_1^{\ 1/3} + A_2^{\ 1/3})\ , \tag{2.17}$$

where R_o is the radius parameter, and A_1 and A_2 are the mass numbers of the emitted particle and the daughter nucleus.

The barrier penetrabilities were calculated with a computer code used by Prof. J. Cerny's group in Lawrence Berkeley Laboratory[9]. In fig. 4 the barrier penetrability for protons and α particles is plotted for each nuclide in the $T_z = -1$, $A = 4n$ series as a function of β-decay energy (see inset). The curves were calculated for the lowest possible ℓ values compatible with an allowed β transition and parity conservation by assuming a constant nuclear radius parameter $R_o = 1.3$ fm. If an effective threshold for particle emission is defined by the condition[1] $P_\ell = 10^{-4}$, then the corresponding upper limit for β-decay energy can be read from fig. 4. Only β transitions of energies lower than this limit lead to observable particle emission. In the decay of ^{20}Na, ^{24}Al, ^{28}P, ^{32}Cl, ^{36}K and ^{40}Sc the limits for proton emission are 0.6, 1.5, 2.2, 3.2, 3.6 and 5.0 MeV and those for α-particle emission are 7.9, 2.3, 2.3, 3.5, 3.3 and 3.7 MeV. A comparison of these figures suggests that α-particle emission should dominate in ^{20}Ne and ^{24}Mg, and compete on equal terms with proton emission in ^{28}Si and ^{32}S. Proton emission should be slightly favoured in ^{36}Ar and predominant in ^{40}Ca. It is evident from fig. 4 that the lower energy limit for proton observation is higher than 0.4 MeV and for observation of α particles higher than 1.0 MeV.

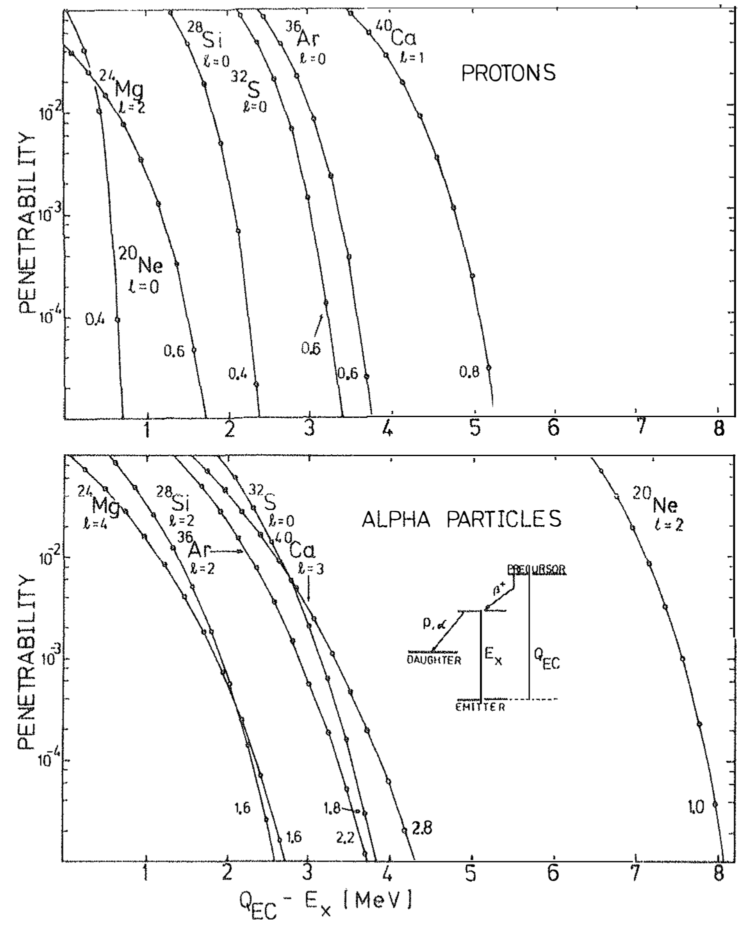

Fig. 4. Barrier penetrabilities for delayed proton and delayed α-particle emission in the $T_z = 0$, $A = 4n$ nuclei. The penetrability is shown for each nuclide as a function of the β-decay energy (see insert). The ℓ values are the minimum values compatible with an allowed β decay and parity conservation. The number in the lower part of each curve gives the particle energy corresponding to the first calculated point on the curve. The energy increment between successive points is 0.2 MeV.

The maximum allowable reduced width is given by the Wigner limit[22]. According to Marion and Young[23] this limit is given by

$$\gamma_W^2 = \frac{3\hbar^2}{2\mu R^2} = \frac{62.70}{\mu R^2} \text{ (MeV)}. \tag{2.18}$$

The dimensionless reduced width

$$\theta^2 = \gamma^2/\gamma_W^2 = \Gamma/2\, P_\ell \gamma_W^2 \tag{2.19}$$

gives the probability of finding a particle in the desired nuclear shell at the nuclear surface. This is closely related to the spectroscopic factor $S = \Gamma/\Gamma_{s.p.} = \gamma^2/\gamma^2_{s.p.}$ obtained in proton or α-particle transfer reactions. In light nuclei there exist[22] clearly defined α cluster or quartet states. The reduced α-particle width of these states is close to the Wigner limit and they are strongly populated in direct α-particle transfer reactions. The reduced α-particle widths are a direct measure of the degree of α clusterization. However, the penetrabilities are strongly dependent on the channel radius and the absolute values of reduced widths cannot be reliably calculated. Instead, comparisons between different levels can be better performed.

3. EXPERIMENTAL METHOD

3.1. Helium-jet transport system

The He-jet technique was used to transfer recoil atoms from the reaction chamber to the measurement site in a low-background area. A small amount of NaCl was introduced into the helium gas by letting it flow through an oven containing NaCl at a temperature of 700 - 800^{o} C. At this temperature the vapour pressure of NaCl is high enough to form clusters. It has been observed[24)] that additives have to form clusters with diameters from 0.01 to 1.0 μm and the concentration should be about $10^5/cm^3$ for efficient transport of activities. In these conditions the obtained transport efficiencies are several tens of per cent.

The target chamber was operated at a pressure of about 0.15 MPa and the pressure in the collection chamber was 400 - 500 Pa. The length of the capillary was varied from 3.0 to 5.4 m and the inner diameter from 1.0 to 1.2 mm. The helium flow rate, normalized to atmospheric pressure, was 30 - 50 cm^3/s. The beam entered the target chamber through a 4.3 mg/cm^2 Ni window. Four targets separated by a distance corresponding to the range of recoil atoms in helium were mounted in the chamber. Also four capillary inlets one for each foil were used. The transmission time through the capillary was measured by a charge-pulse method using slow pulsing of the proton beam and a charge collector in the collecting chamber. An average transmission time for a capillary, 5.4 m long and 1.2 mm in inner diameter, was measured to be 80 - 100 ms.

The collection chamber and the location of the detectors and the capillary are shown in fig. 5. The reaction products were deposited onto an aluminized mylar tape, which could be programmed to move periodically from a collection position to various detection positions according to a preselected time schedule. The capillary could be placed either in position 1 or 2. The position 1 was used in branching ratio measurements, when the Ge(Li) detector had to be shielded from the radiation of the collection point. In addition, the Ge(Li) detector was blocked off during the tape movement. The distance of the particle detector and the capillary outlet from the tape was 0.5 - 1.0 cm.

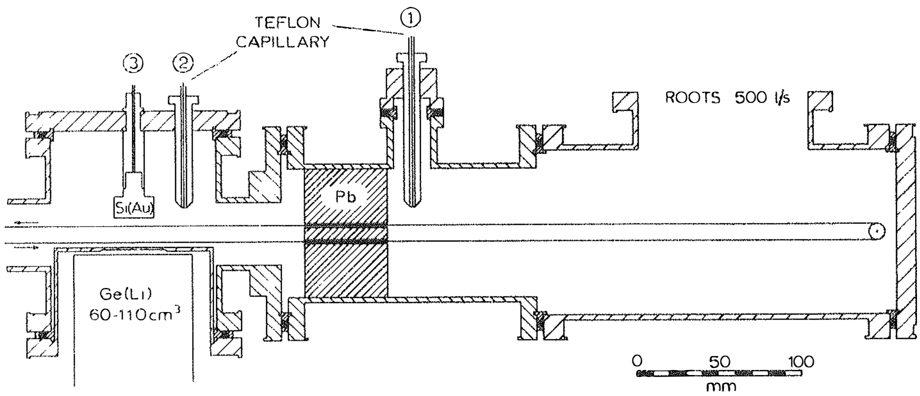

Fig. 5. A schematic presentation of the collecting chamber.

3.2. Delayed particle detection

Because the beta branching to particle emitting levels is very weak in the nuclides under study the intense β background caused by β decay to other levels seriously interfered with the detection of delayed particles. The β continuum was reduced by using thin surface-barrier detectors. The detectors ranged in thickness from 13.9 μm to 100 μm. The 100 μm detectors were partially depleted while the thinner ones were totally depleted. In many experiments the sensitive volume of the 100 μm detector was reduced by using lower than optimum bias voltage. In this way the intense background caused by multiple β scattering in the detector was substantially reduced.

Maximum energy losses for protons and α particles in the various detectors are shown in table 1. Protons of energies higher than 0.9 MeV lose only a part of their energy in passing through the 13.9 μm detector while α particles up to 3.5 MeV show up at their full energy. Thus, a comparison of spectra measured with the 13.9 μm and 100 μm detectors provides a means for making a clear distinction between proton and α-particle groups for energies higher than 0.9 MeV. However, because emission of α particles is suppressed more severely than proton emission by the Coulomb barrier, the lowest groups are due to protons. This was confirmed by using a 50 $\mu g/cm^2$ polyethene absorber foil in front of the detector, which shifted α peaks by 100 - 150 keV but proton peaks only by 10 - 20 keV.

Table 1. Properties of Si(Au) surface-barrier detectors

Thickness (μm)	Maximum energy loss (MeV) protons	α particles
13.9	0.9	3.5
26	1.4	5.1
31.1	1.6	6.0
100	3.1	12

Half-life measurements were carried out using the signal indicating the completion of a tape cycle as time reference. In these experiments the pulses from the detector were stored on a magnetic tape in an event-by-event mode. An off-line analysis was subsequently made with gates set on either the time or the energy axis.

The observed width of the delayed particle groups is influenced by the capacitance of the detector and the thickness of the source. Also the momentum broadening due to the preceding β decay and the intrinsic width of the particle emitting level affect the resolution. Since the capacitance of a detector is proportional to the ratio of area to thickness, the thin detectors have high capacitive noise which lowers the resolution. The thickness of the source depends on the rate at which NaCl emerges from the capillary. Because the nuclei under study are all short lived, the measured rate of (1.0 ± 0.5) μg/s, did not notably hamper the resolution. In the decay of ^{20}Na β energies to unbound states are high and the mass of the daughter nucleus is small, the β broadening may range up to 40 keV. For other nuclei under study this broadening is estimated to contribute less than 15 keV to the peak width.

3.3. Particle branching ratio measurements

The particle branchings pro β decay were determined by comparing the delayed spectrum to a simultaneously measured γ-ray spectrum. The efficiency of the γ-ray detector relative to the particle detector was determined by comparing the intensity of the 6.28 MeV α-particle group of ^{211}Bi to that of the succeeding 351 keV γ transition in ^{207}Tl. The internal conversion coefficient[25)] of the 351 keV transition was taken to be 0.24. ^{211}Bi was collected from a ^{227}Ac source and deposited onto the tape in the same way as the activities from the target chamber. The energy dependence of the Ge(Li) detector efficiency was measured in the same geometry using well-known standard γ sources. The γ transitions and intensities used for each nuclide in branching ratio measurements are shown in table 2.

Table 2. Gamma-transition energies and intensities used in particle branching ratio studies

Nuclide	E_γ (keV)	intensity (%)	ref.
^{20}Na	1633	79.2 ± 1.6	26
^{24m}Al	426	82.5 ± 3.1	27
^{24}Al	1077	14.5 ± 0.7	27, 28
^{28}P	1778	95.5 ± 0.5	29
^{32}Cl	2231	92 ± 4	30
^{36}K	1970	79 ± 8	31
^{40}Sc	755	41 ± 4	30

4. RESULTS AND DISCUSSION

4.1. Decay of ^{20}Na

The radioactive ^{20}Na was produced by bombarding ^{20}Ne with 20 MeV protons. A neon target was obtained by mixing neon gas (^{20}Ne 90.5 %) into the helium flow. The partial neon density in the gas flow was 8 - 16 $\mu g/cm^3$.

A delayed particle spectrum of ^{20}Na measured with the 100 μm detector is shown in fig. 6. Nine α-particle groups are seen in the energy range 2.0 - 6.6 MeV. The low energy peaks are due to ^{16}O recoils that correspond to the α-particle groups. The weak group at 1.58 MeV energy probably arises from summation of recoil events. A sum peak of the two most intense α-particle groups is seen at 6.52 MeV.

The energy calibration was done using the well-known energies of the α-decaying levels at 7421 ± 1 keV and 10272 ± 2 keV and the α-particle binding energy B_α = 4730.9 ± 0.5 keV in ^{20}Ne[32]. These values result in alpha energies of 2152 and 4433 keV. The α-particle branching ratios were measured by comparing the particle spectrum to a simultaneously measured γ-ray spectrum as described in the experimental section. The energies and intensities of the particle groups are listed in table 3. These results agree within error limits with the previously measured values by Torgerson et al.[5].

Log ft values were calculated using Q_{EC} = 13887 ± 7 keV and $T_{1/2}$ = 446 ± 5 ms for ^{20}Na[32] and the log f tables of Gove and Martin[19]. The beta intensities were taken to be equal to α branchings except for the 10.27 MeV state for which the γ width is not negligible as compared with the α width[32].

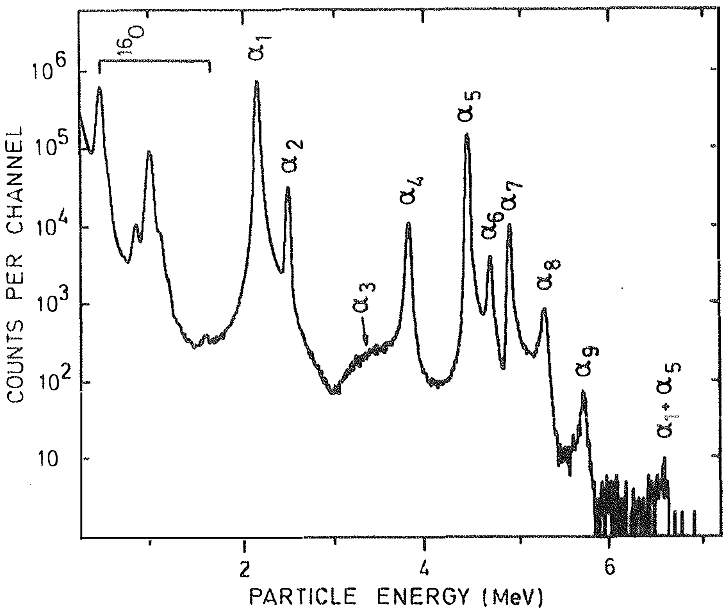

Fig. 6. Delayed α-particle spectrum of ^{20}Na measured with the 100 μm Si(Au) detector. The peaks below 1.6 MeV are due to ^{16}O recoils. The collecting and measuring period was 300 ms and the integrated beam current 17 mC.

Allowed β transitions from the ground state of ^{20}Na ($J^\pi = 2^+$) populate levels in ^{20}Ne which have $J^\pi = 1^+$, 2^+ and 3^+. Alpha decay to the ground state of ^{16}O ($J^\pi = 0^+$) is expected only from 2^+ states, because the transitions from 1^+ and 3^+ states are strongly hindered as parity forbidden. This restriction is no longer valid above E_x = 10.861 MeV since α decay to the 6.130 MeV $J^\pi = 3^-$ state in ^{16}O becomes energetically possible. However, taking into account the inhibitive effect of the Coulomb barrier, α transitions to this state are not expected to take place below 12 MeV excitations. Because the proton binding energy is B_p = 12.85 MeV in ^{20}Ne, 1^+ and 3^+ states below E_x = 12 MeV can only decay by γ emission. As is seen from table 3 all observed β transitions are of the allowed type and therefore the spin and parity of the α-decaying levels is 2^+. This is in agreement with the spin and parity values determined in resonance reaction studies.

In table 3 the experimental log ft values have been compared with shell-model predictions of Brown and Wildenthal[11]. They used a complete sd-shell space for the four nucleons outside the ^{16}O core. The values calculated for $J^\pi = 2^+$ states with empirical single-particle matrix elements[33] have been included in table 3. The agreement is quite good for the transitions to the 7.42, 10.27 and 10.58 MeV levels. A predicted strong transition at 11.53 MeV with a log ft = 3.78 cannot be clearly identified. The best agreement is obtained with the 10.84 MeV level. It is possible that the β strength is divided over the three states between 10.8 - 11.9 MeV. The total β-transition strength of these states corresponds to a log ft value of 4.0, but a part of the calculated β strength is still missing. This may indicate a still stronger configuration mixing. At these high energies excitations into the fp shell are becoming important components of these states. The broad 8.8 MeV 2^+ state has been interpreted by Fortune et al.[34] as due to the mixing of a dominantly sd-shell state and a state with at least two fp-shell particles. The 7.83 MeV state is proposed[35] to arise from excitations including eight sd-shell nucleons outside a ^{12}C core. The calculated β strength may then be distributed over these states. If the transition to the 10.27 MeV level is excluded, the experimental β strength to unbound states corresponds to a total log ft value of 3.70 which is in good agreement with the calculated value of 3.66.

Table 3. Summary of delayed α-particle emission of ^{20}Na

	E_α (keV)	FWHM (keV)	E_x in ^{20}Ne (keV) this work	E_x in ^{20}Ne (keV) previous[a]	I_α (%)	log ft	E_x^{calc}[b] (keV)	log ft_{calc}[b]
α_1	2152±1[c]	48	7421	7421.4± 1.0	16.1 ±1.5	4.19±0.04	7370	4.41
α_2	2479±2	46	7830	7829 ± 2	0.68 ±0.07	5.41±0.05		
α_3	3500±200	700	9100	≈8.8	0.050 ±0.007	6.0 ±0.2		
α_4	3800±5	52	9481	9493 ±10	0.262 ±0.030	5.03±0.05		
α_5	4433±2[c]	41	10272	10272.4± 2.0	2.83 ±0.26	3.47±0.04[d]	10130	3.468
α_6	4676±5	54	10576	10583 ± 6	0.090 ±0.010	4.75±0.05	10230	4.90
α_7	4887±3	38	10840	10840 ± 5	0.178 ±0.020	4.21±0.05		
α_8	5256±6	68	11301	11322 ± 7	0.028 ±0.005	4.53±0.08	11530	3.78
α_9	5687±8	70	11840	11866 ± 9	0.0016±0.0003	5.01±0.09		

a) Ref. 32

b) Ref. 11

c) Used for calibration

d) Γ_α/Γ = 0.964±0.006

The low log ft value for the transition to the 10.27 MeV state shows it to be superallowed and thus the 10.27 MeV state to be the analog of the ^{20}Na ground state. In accordance with β-decay selection rules both Fermi and Gamow-Teller transitions are possible between these states. Alpha transitions from the T = 1 analog state are only possible if it contains admixtures of T = 0 states. The peak shapes of the delayed α-particle groups depend on the β^+, ν and α angular correlations in the decay process. These correlations depend on the β-decay form factors which are different for Fermi and Gamow-Teller decay. Macfarlane et al.[36)] have studied the discussed angular correlation in the decay of ^{20}Na. Their results indicate that the Fermi component of the β transition to the analog state is 84 ± 7 %. Recently Clifford et al.[37)] have carried out a more detailed investigation making coincidence measurements between the delayed α particles and the positrons. Their results indicate 9 ± 5 % T = 0 mixing in the analog state. They have also measured very accurately the β branching to the analog state which yields a log ft value of 3.476 ± 0.009. Using these values and an estimated radiative correction δ_R = 1.61 %[12)] the Gamow-Teller matrix element is calculated from equation (2.2) to be $|\langle\sigma\,\tau\rangle|_{exp}$ = 0.37 ± 0.05. This agrees well with the value $|\langle\sigma\,\tau\rangle|_{calc}$ = 0.326 calculated by the shell model[11)]. Clifford et al. have also deduced upper limits for the charge dependent mixing of levels with analog state for five levels. For the levels at 7.42, 7.83 and 9.48 MeV they obtained the mixing to be ≤ 0.3, ≤ 0.07 and ≤ 0.4 %. Because 0.4 % isospin mixing corresponds to a log ft = 5.9 for a pure Fermi transition, the β transitions to the 7 - 9.5 MeV states cannot be fully due to isospin mixing. For the 10.58 and 10.84 MeV levels Clifford et al. deduced that the mixing is less than 4.2 and 7.8 %, respectively.

The properties of ^{20}Ne levels decaying by delayed α-particle emission are given in table 4. The partial Γ_α and Γ_γ widths were taken from the compilation Ajzenberg - Selove[32]. The measured widths (FWHM) of the α groups are given in table 3. Although the experimental resolution of the detector was about 15 keV the measured peak widths are about 40 keV or more. This spreading is mainly due to the momentum broadening caused by the preceding β decay, which can be calculated to contribute from 20 to 40 keV to the width. Also the intrinsic width is large enough for several levels in ^{20}Ne to contribute notably to the experimental width.

The reduced widths $\theta_\alpha^2 = \gamma_\alpha^2/\gamma_w^2$ in table 4 were deduced from the α widths by using the Wigner limit of $\gamma_w^2 = 690$ keV. The reduced widths are about 1 % of the Wigner width except for the states at 7.42 and 9.1 MeV and for the 10.27 MeV analog state. The appreciably large α widths cannot be explained by the shell model. Tomoda and Arima[38] have successfully combined the shell model and the α-cluster model in ^{20}Ne. They analyzed the wave functions of some 0^+ rotational bands and concluded that the 7.42 and 8.8 MeV 2^+ states should contain an 11 and 71 % α-cluster component in their total wave function. This is in agreement with the reduced widths calculated in table 4. The reduced α width of the 10.27 MeV state is two orders of magnitude lower than those of the nearby states. This indicates that the α decay from the analog state is strongly hindered.

Table 4. Properties of ^{20}Ne levels decaying by delayed alpha-particle emission

E_x (MeV)	$J^{\pi};T$	Γ_{α} [a] (keV)	Γ_{γ} [a] (eV)	P_{ℓ}	θ_{α}^{2} [b] (%)
7.42	$2^+;0$	8	0.03	0.085	6.8
7.83	$2^+;0$	2.4	0.07	0.21	0.83
9.10	$2^+;0$	$\geq$800		0.87	67
9.48	$2^+;0$	24	0.26	1.2	1.4
10.27	$2^+;1+0$	0.12±0.02	4.3±0.2	1.8	0.0048
10.58	$2^+;0$	24		2.1	0.83
10.84	$2^+;0$	13		2.3	0.41
11.30	$2^+;0$	40		2.6	1.1
11.84	$2^+;0$	46		2.9	1.1

a) Ref. 32

b) $\theta_{\alpha}^{2} = \Gamma_{\alpha}/2P_{\ell}\gamma_{W}^{2}$, $\gamma_{W}^{2} = 690$ keV

4.2. Decay of ^{24}Al and ^{24m}Al

Delayed particle spectra derived from irradiation of natural Mg (^{24}Mg 78.9 %) targets are displayed in figs. 7 and 8. The spectrum in fig. 7 (a) was measured with the 100 μm detector using consecutive 200 ms collecting and measuring cycles. The spectrum (b) was measured with a timing scheme consisting of one second collecting and measuring cycles separated by an interval of one second. This timing allowed the 129 ms isomeric state to decay and the spectrum displays only peaks assigned to the decay of the 2.07 s ground state. The peaks associated with the decay of ^{24m}Al and ^{24}Al are marked by (m) and (g), respectively. It was found that some weak groups in the spectrum of fig. 7 (a) arise from sulphur that was evaporated on the Mg targets during the calibration procedure. Such peaks have been marked by (Cl) according to the precursor nuclide ^{32}Cl. In the spectra taken with the 100 μm detector positron background extends up to 1 MeV. In the spectrum measured with the 13.9 μm detector it is significant only for energies below 0.5 MeV, as can be seen in fig. 8. However, no new particle groups are evident in the energy range 0.5 – 1.0 MeV. Because the thickness of the 13.9 μm detector corresponds to a maximum energy loss of about 900 keV for protons, all particle groups were assigned due to α particles. This result was confirmed by energy-degradation measurements.

The energy calibration of the delayed particle spectra is based on the assignment of the particle groups at 1421 and 1985 keV to α decay from the 11018 and 11694 keV levels in ^{24}Mg and on the α-particle binding energy B_α = 9312.5 ± 0.8 keV[39]. Both levels are well established by α-resonance reaction studies and are well separated from any other known levels in ^{24}Mg. The results concerning the decay of ^{24}Al and ^{24m}Al to particle emitting levels

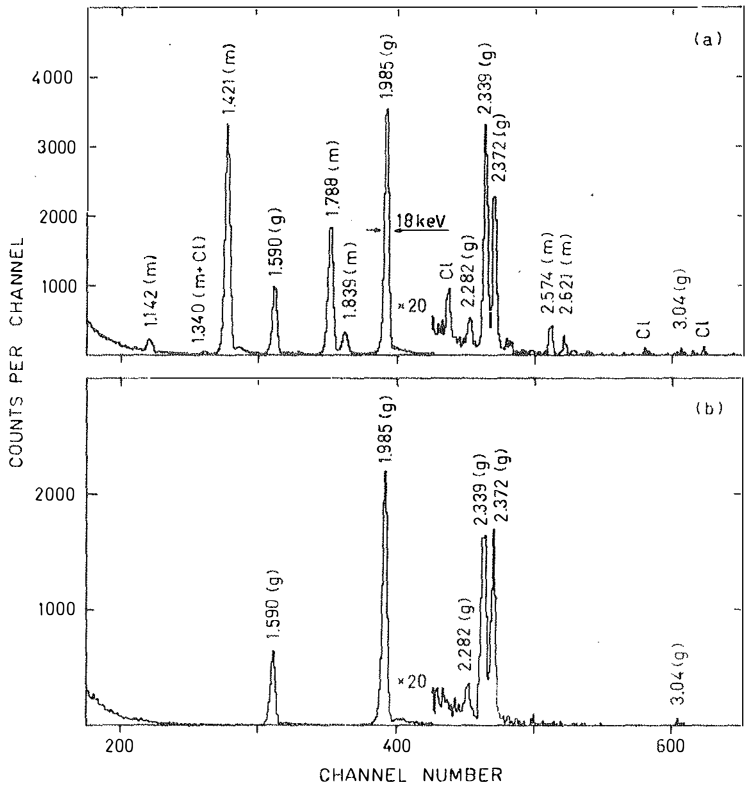

Fig. 7. Delayed α-particle spectra of ^{24}Al and ^{24m}Al measured with the 100 μm detector. The collecting and measuring period was 200 ms for spectrum (a) and 1 s for spectrum (b). In (a) the two cycles were consecutive, but in (b) they were separated by an interval of one second. The integrated beam current was 80 mC for spectrum (a) and 18 mC for spectrum (b). The peaks marked with (m) and (g) were associated with the decay of ^{24m}Al and ^{24}Al, respectively.

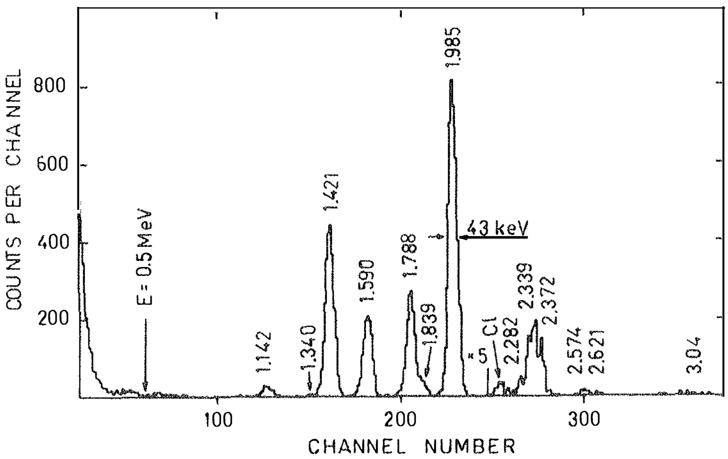

Fig. 8. Delayed α-particle spectrum measured with the 13.9 μm detector. The collecting and measuring period was 300 ms and the integrated beam current 17 mC.

in ^{24}Mg are summarized in tables 5 and 6. The measured intensities for ^{24}Al are higher than those reported by Steigerwalt et al.[6)] by a factor of approximately five. In a later study of Torgerson et al.[7)] five α transitions were assigned to the decay of ^{24}Al and three to the decay of ^{24m}Al, but the absolute particle branchings were not determined.

In tables 5 and 6 each observed α-particle emitting level has been matched with a known resonance level on the basis of energy compatibility and a spin and parity assignment consistent with an allowed β-decay of the precursor. Alpha transitions associated with the decay of ^{24}Al ($J^\pi = 4^+$) are only expected from 4^+ states while in the case of ^{24m}Al ($J^\pi = 1^+$) the α transitions are expected to take place from 0^+ or 2^+ states. All the levels in table 5 have been characterized as 4^+ states on the basis of angular distribution measured in resonance studies[39)]. The levels in table 6 have been assigned $J^\pi = 2^+$ except for the levels at 10680 and 11456 keV with $J^\pi = 0^+$ assignments. Both 11455 ($J^\pi = 2^+$) and 11456 ($J^\pi = 0^+$) keV levels could correspond to the α-particle group at 1788 keV in terms of energy.

Table 5. Summary of delayed α-particle emission of ^{24}Al

	E_α (keV)	E_x in ^{24}Mg (keV) this work	E_x in ^{24}Mg (keV) previous[a]	$J^\pi;T$[a]	I_α $\times 10^{-6}$	log ft	E_x calc[b] (keV)	$J^\pi;0$[b]	log ft calc[b]	log ft calc[c]
α_1	1590± 5	11221	11217±3	$4^+;0$	72 ±20	5.9±0.1[e]	11150	$4^+;0$	5.26	5.16
α_2	1985± 4[d]	11694	11694±3	$4^+;0$	260 ±60	4.7±0.1[e]	12180	$4^+;0$	4.35	4.10
α_3	2282± 5	12051	12049±1	$4^+;0$	1.1± 0.3	6.4±0.1	12630	$4^+;0$	5.91	6.54
α_4	2339± 5	12119	12119±5	$4^+;0$	10 ± 3	5.3±0.1	12240	$4^+;0$	5.23	5.15
α_5	2372± 5	12159	12159±3	$4^+;0$	7.5± 2.0	5.3±0.1				
α_6	3040±10	12961	12965±1	$4^+;0$	0.2± 0.1	5.3±0.3 (EC)				

a) Refs. 39,42

b) Ref. 11

c) Ref. 40

d) Used for calibration

e) Upper limit (see table 7)

Table 6. Summary of delayed α-particle emission of ^{24m}Al

	E_α (keV)	E_x in ^{24}Mg (keV) this work	E_x in ^{24}Mg (keV) previous[a)]	$J^\pi;T$[a)]	I_α ($\times 10^{-6}$)	log ft	E_x^{calc}[b)] (keV)	$J^\pi;T$[b)]	log ft^{calc}[b)]
α_1	1142±5	10683	10680 ±3	$0^+;0$	9 ± 3	6.4±0.1[d)]	9770	$0^+;0$	6.63
α_2	1340±8	10921	10922 ±3	$2^+;0$	0.9± 0.4	7.3±0.1[d)]	10340 10970	$2^+;0$ $2^+;0$	6.24 5.92
α_3	1421±3[c)]	11018	11018 ±2	$2^+;0$	160 ±50	4.9±0.1[d)]	11540	$2^+;0$	4.39
α_4	1788±5	11458	11453 ±5 11456 ±5	$2^+;0$ $0^+;0$	92 ±30	4.7±0.1[d)]	12690 11790	$2^+;0$ $0^+;0$	4.67 8.85
α_5	1839±8	11519	11520 ±3	$2^+;0$	17 ± 6	5.4±0.1	12860	$2^+;0$	5.33
α_6	2574±5	12401	12402.5±0.8	$2^+;0$	0.8± 0.3	5.5±0.1	12940	$2^+;0$	5.35
α_7	2621±8	12458	12465 ±3	$2^+;0$	0.4± 0.2	5.7±0.3			

a) Ref. 39

b) Ref. 11

c) Used for calibration

d) Upper limit (see table 7)

Log ft values were determined using the known total decay energy of 13878.3 ± 3.9 keV[39] for ^{24}Al. The decay energy of ^{24m}Al was obtained with the help of the measured energy 425.8 ± 0.1 keV for the isomeric transition[27,41]. The partial half-lives were calculated assuming the α branchings to be equal to β intensities. The experimental log ft values were compared with the shell-model predictions tabulated by Brown and Wildenthal[11]. All the natural parity states with T = 0 were included in tables 5 and 6. Kelvin et al.[40] have also calculated log ft values for ^{24}Al β transitions using the same Chung - Wildenthal interaction but with somewhat different matrix elements. These values are shown in table 5 for the four transitions to 4^+ levels. A strong transition has been predicted to a 12.18 MeV 4^+ level with predicted log ft values of 4.35 and 4.10. The strongest observed β transition populates the 11.69 MeV level and has a log ft $\leq$ 4.7. A good compatibility in log ft values is obtained, if the transition to the predicted 12.63 MeV level is associated with the 12.05 MeV level and the transition to a 12.24 MeV level is associated with the close-lying 12.12 and 12.16 MeV levels. The 12.96 MeV level is excluded because it can only be populated by electron capture. In the case of ^{24m}Al eight β transitions to 0^+ or 2^+ levels have been predicted in the energy range corresponding to delayed particle emission. At 11.46 MeV there are two possible resonance levels to be populated in β decay of ^{24m}Al. The observed log ft value 4.7 is consistent with the predicted value of 4.67 for the 2^+ state at 12.69 MeV but inconsistent with the value 8.85 for the 0^+ state of 11.79 MeV energy. The calculated β strength for the 12.94 MeV level seems to be distributed over the close-lying levels at 12.40 and 12.46 MeV. The total β strength corresponding to a log ft value of 5.3 is in good agreement with the calculated value 5.35.

Unnatural parity states decay by proton or γ-ray emission. Although the proton binding energy[39] B_p = 11.690 MeV in ^{24}Mg is well below the β-decay energy, no proton groups were observed. If the counts between 0.5 - 1.0 MeV in the spectrum of fig. 8 are assumed to be due to protons, an upper limit for the total proton intensity can be estimated to be less than $8\cdot10^{-6}$ in both ^{24}Al and ^{24m}Al decays. Shell-model calculations predict eleven β transitions to levels above 12 MeV, which are forbidden against α decay. However, the β intensities are suggested to be very weak and there are only two transitions which would be above the proton detection limit. In the decay of ^{24}Al a transition to a $J^{\pi} = 3^{+}$, T = 0 level at 12.01 MeV with log ft = 5.00 and in the decay of ^{24m}Al a transition to a $J^{\pi} = 2^{+}$, T = 1 level at 12.65 with log ft 5.06 have been proposed[11]. These predictions result in branchings of about 10^{-5}, but the branchings are very sensitive to the calculated level energies.

The properties of the ^{24}Mg levels observed in delayed α-particle emission are given in table 7. The reduced α widths were determined from the known level widths by assuming $\Gamma_{\alpha} >> \Gamma_{\gamma}$. Thus the γ widths can be estimated from the measured resonance strengths $S(\alpha,\gamma) = (2J + 1)\Gamma_{\alpha}\Gamma_{\gamma}/\Gamma \approx (2J + 1)\Gamma_{\gamma}$. Rotational bands are better developed in ^{24}Mg than in any other sd-shell nucleus and cluster-model calculations give a good account with experiments. The low-lying states can be ascribed to three rotational bands with $K^{\pi} = 0_1^{+}$, 2_1^{+} and 0_2^{+} [42]. The levels at 11.22 or 11.69 MeV are the most possible candidates for the 4^{+} member of the 0_2^{+} band[43]. The reduced widths (in table 7) are large for many levels populated in β decay of ^{24}Al. Especially the 12.12 MeV state has a reduced width close to the Wigner limit. This state is also quite strongly excited in the $^{12}C(^{16}O,\alpha)^{24}Mg$ reaction[44] which strongly populates α-cluster or four nucleon states.

Table 7. Properties of ^{24}Mg levels decaying by delayed alpha-particle emission

E_x (MeV)	J^{π}	Γ_{α} a) (eV)	Γ_{γ} a,b) (eV)	P_{ℓ} ($\times 10^{-3}$)	θ_{α}^2 c) (%)
10.68	0^+	>1.2	$\geq$0.3	0.039	>2.6
10.92	2^+	>2.4	$\geq$0.6	0.060	>3.3
11.02	2^+	>1.5	$\geq$0.4	0.13	>1.0
11.22	4^+	>1.1	$\geq$0.3	0.015	>6.1
11.46	2^+	>1.3	$\geq$0.3	2.0	>0.05
11.46	0^+	1000		9.5	8.8
11.52	2^+	500	0.20	2.7	15
11.69	4^+	>0.3	$\geq$0.1	0.23	>0.11
12.05	4^+	6.5 d)		1.1	0.49
12.12	4^+	1900 d)		1.4	113
12.16	4^+	900 d)	0.64	1.6	47
12.40	2^+	<100		63	<0.13
12.46	2^+	3800 d)	0.46	73	4.3
12.96	4^+	3300 d)		18	15

a) Ref. 39

b) $\Gamma_{\gamma} \geqq S(\alpha,\gamma)/(2J+1)$

c) $\gamma_W^2 = 600$ keV

d) Ref. 42

4.3. Decay of ^{28}P

Targets of natural silicon (^{28}Si 92.2 %) were used for the production of ^{28}P. They were prepared by sputtering 0.2 mg/cm^2 of pure silicon onto an aluminium foil. Since argon ions were used in the sputtering process subsequent purity analysis based on proton back scattering revealed (4 ± 1) % by weight of argon in the targets. Delayed particle spectra resulting from proton bombardments of these targets are displayed in figs. 9 and 10. The spectra displayed in fig. 9 (a) and (b) were measured with the 100 μm and the 13.9 μm detectors, respectively. A comparison of these spectra shows clearly that ^{28}P is a precursor of both delayed α particles and delayed protons. Because the ten groups above 1 MeV show up in equal position in both spectra, they are due to α particles. The Coulomb barrier is prohibitively high when $E_\alpha \leq 1$ MeV and thus the groups at lower energy must be proton induced. This was confirmed for the 680 keV peak by absorption measurements. In the spectrum measured with the 100 μm detector proton groups are seen at 0.953, 1.102 and 1.269 MeV. These groups contribute a broad distribution of counts between 0.5 and 0.9 MeV to the spectrum measured with the 13.9 μm detector, which makes the observation of underlying details uncertain. This part of the spectrum was measured by mounting the 13.9 μm detector, at 45° angle in front of the source, which allowed protons up to 1.2 MeV to be absorbed in the detector[45]. A measurement with a better counting statistics was recently carried out using the 31.1 μm detector. In this spectrum displayed in fig. 10 the first proton group at 0.458 MeV was partly hidden under the β continuum.

The energy calibration was made by assigning several of the observed groups to levels, whose energies have been accurately measured[39]. In the determination of level energies and log ft values B_p = 11585.96 ± 0.26 keV

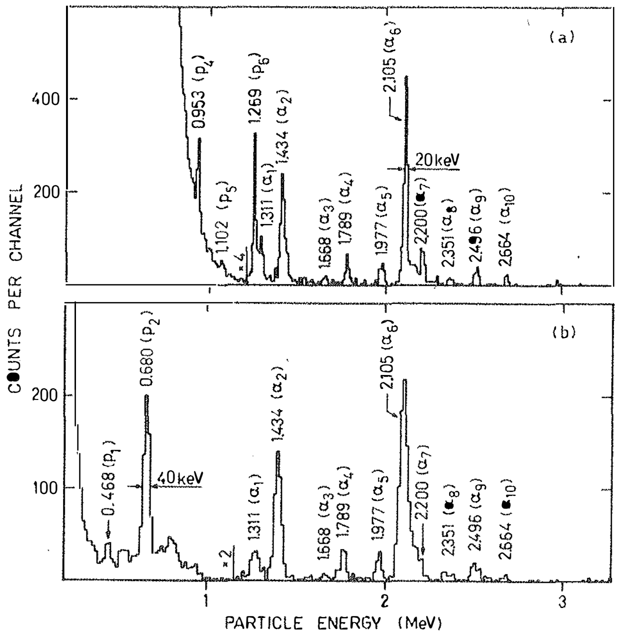

Fig. 9. Delayed particle spectra of ^{28}P measured with the 100 μm (a) and 13.9 μm (b) detectors. The collecting and measuring period was 500 ms for spectrum (a) and 300 ms for spectrum (b) and the corresponding integrated beam currents were 75 mC and 85 mC.

and B_{α} = 9985.56 ± 0.36 keV were used for ^{28}Si and Q_{EC} = 14331.7 ± 3.7 keV and $T_{1/2}$ = 270.0 ± 0.5 ms for ^{28}P[39]. Protons and α particles were calibrated separately. The energy difference between these two calibrations was about 10 keV being mainly due to the energy loss difference in the gold electrode of the surface barrier detector. Energies and intensities of the observed particle groups with other related information are given in table 8. The log ft values were calculated by taking into account proton, α-particle and γ-ray widths. The ratios of γ width to total width were calculated from the resonance yields as shown in table 9.

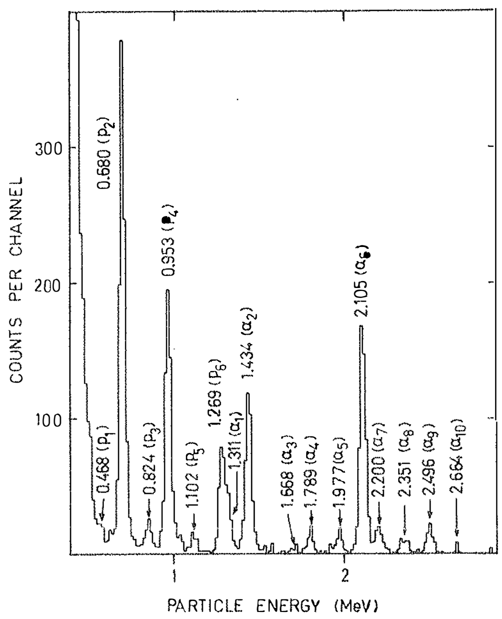

Fig. 10. Delayed particle spectrum of ^{28}P measured with the 31.1 μm detector. The collecting and measuring period was 600 ms and the integrated beam current 60 mC.

The assignment of an observed particle group to a specific resonance level is based mainly on energy compatibility and on the spin and parity values restricted by β-decay selection rules. A weak proton group at 1.10 MeV was earlier[44] assigned to a $J^{\pi} = (1, 2^{+})$, T = 1 level at 12.716 MeV. Because this level is the only candidate[46] for the analog of the 3.54 MeV 1^{+} state in ^{28}Al, it is not expected to be populated by allowed β decay from ^{28}P ground state ($J^{\pi} = 3^{+}$). On the other hand, the assignment of the 1.10 MeV proton group to a 2^{+} level at 12.727 MeV is supported by an energy measurement made with the 31.1 μm detector. The level at 12.57 MeV has a previous assignment $J^{\pi} = 2$. The selection rules

Table 8. Summary of delayed particle emission of ^{28}P

	particle energy (keV)	E_x in ^{28}Si (keV) this work	E_x in ^{28}Si (keV) previous[a)]	$J^{\pi};T$[a)]	I_p ($\times 10^{-6}$)	I_{α} ($\times 10^{-6}$)	Γ_{γ}/Γ[b)] (%)	log ft
p_1	468±10	12071	12072.7±0.3	$2^+;0$	0.5 ±0.2	0.34±0.11	11	6.3±0.2
p_2	680± 2[c)]	12291	12291.0±0.3	$2^+;0$	5.7 ±1.3	0.37±0.12	1.1	5.2±0.1
p_3	824± 6	12441	12441.8±0.3	$2^+;0$	0.32±0.13	3.1 ±0.7	1.6	5.1±0.1
p_4	953± 2[c)]	12574	12574.3±0.3	$2^+;1$[f)]	3.4 ±0.8	≤0.3		≤4.9±0.1
p_5	1102± 6	12729	12726.8±0.3	$2^+;0$	0.29±0.10	0.23±0.008	0.04	5.3±0.2
p_6	1269± 8	12902	12900.9±0.3	$2^+;0$	1.3 ±0.4	0.40±0.13	0.4	4.4±0.1
α_1	1311±12	11515	11516.7±0.4	$2^+;0$		0.74±0.26		≤7.1±0.2
α_2	1434± 2[c)]	11659	11658.0±0.5	$2^+;0$		2.3 ±0.6		≤6.5±0.1
α_3	1668± 5	11932	11933 ±3	$2^+,3^-,4^+;0$[f)]		0.10±0.05		≤7.5±0.2
α_4	1789± 5	12073	12072.7±0.3	$2^+;0$	0.6 ±0.3	0.34±0.11	11	6.3±0.2
α_5	1977± 5	12292	12291.0±0.3	$2^+;0$	5.7 ±1.3	0.37±0.12	1.1	5.2±0.1
α_6	2105± 2[c)]	12441	12441.8±0.3	$2^+;0$	0.42±0.13	3.1 ±0.7	1.6	5.1±0.1
α_7	2200± 5	12552	12551.8±0.3	$4^+;0$	≤0.5	0.48±0.15	8	5.5±0.2[d)]
α_8	2351± 5	12728	12726.8±0.3	$2^+;0$	0.29±0.10	0.23±0.08	0.04	5.3±0.2
α_9	2496± 5	12898	12900.9±0.3	$2^+;0$	1.3 ±0.4	0.40±0.13	0.4	4.4±0.1
α_{10}	2664± 5	13094	13094.6±0.3	$4^+;0$	≤0.4	0.10±0.06	0.2	5.1±0.3[e)]

a) Ref. 39 , b) See table 9, c) Used for calibration, d) Γ_{α}/Γ_p = 1.3, see table 9, e) Γ_{α}/Γ_p = 3.6, see table 9

f) Partly or totally from this work

for β decay indicate a positive parity for this level. This is expected also because this level is likely to be the T = 1 analog of the 3.35 MeV 2^+ level in ^{28}Al[39]. The weak α group at 1.668 MeV was assigned to a 11.03 MeV level. The spin and parity of this state were not determined but β-decay and α-decay selection rules indicate 2^+, 3^- or 4^+ for this level.

According to the penetrability calculations particle transitions populating excited states in either of the daughter nuclides are energetically very unfavoured compared to the ground state transitions. Thus a transition populating an excited state should also be accompanied with a transition leading to the ground state. Exceptions are α transitions from unnatural parity states 3^+ which are allowed to the 2^+ excited state but parity forbidden to the 0^+ ground state. It cannot be excluded that the weak 1.67 MeV α group arises from this kind of transition although no suitable resonance level is known at corresponding excitation. For the other groups the population of the first excited state would imply prohibitively small log ft values. Besides this the energies of the delayed particle groups are compatible with a known resonance as indicated in table 8. All the observed proton and α-particle groups have been therefore assigned to transitions leading to the ground state.

Proton decay was observed only from 2^+ states. Seven of the observed α transitions originate from 2^+ levels and two from 4^+ levels. In the studied energy range there are[39] only two uniquely assigned 2^+ resonance states but several 3^+ and 4^+ states which were not observed. Shell-model calculations for log ft values were not available. This is possibly due to the fact that ^{28}Si is located in the middle of the sd shell, where the matrix dimensions are maximal.

Properties of ^{28}Si levels decaying via delayed particle emission are shown in table 9. In cases where proton and α-particle emission were observed from the same level, the ratio of partial widths Γ_α/Γ_p was determined from the peak areas. In other cases an upper limit was deduced from the background of the spectra. The partial width ratio can also be deduced from the resonance strengths $\Gamma_\alpha/\Gamma_p = S(\alpha,\gamma) / S(p,\gamma)$. In table 9 these ratios were calculated from the (α,γ) data of Maas et al.[47] and the (p,γ) data of Meyer et al.[48]. The errors in the strengths are estimated to be 20 % in the (α,γ) work and 30 % in the (p,γ) work. The errors in observed peak areas were taken to be statistical. Meyer et al. normalized their (p,γ) strengths to an E_p = 632 keV resonance, the strength of which has later been shown[49] to be 60 % too high. This correction has been taken into account in table 9. The agreement with the resonance data is very good except for the 12.44 and 12.73 MeV levels. Tveter[50] has deduced the proton width of the 12.73 MeV level to be $\Gamma_p/\Gamma = 0.42 \pm 0.06$ using a (p, p_0) reaction. Assuming the γ width to be negligible a partial width ratio $\Gamma_\alpha/\Gamma_p = 1.4$ can be deduced from this value, which is in better agreement with our measurement.

In principle there are three open decay channels, i.e. proton, α-particle and γ-ray emission, for the levels under consideration. If the resonances have been excited through the three reactions (p,γ), (α,γ) and (p, α_0), unique determinations of partial widths can be obtained from the measured yields. The partial widths can also be calculated from the (p, α_0) and (α,γ) yield, if the partial width ratio Γ_α/Γ_p can be determined from the delayed particle spectrum.

The partial widths were calculated by using the observed partial width ratios and the resonance yields. The partial widths for the 12.90 MeV level were derived from the measured total width $\Gamma = 250 \pm 30$ eV[50]. The total width has been measured by the blocking technique to be 11 ± 2 eV[51] and 28 ± 10 eV[52] for the 12.29 MeV level and 24 ± 3 eV[53] and 17 ± 5 eV[54]

Table 9. Properties of ^{28}Si levels decaying by delayed proton emission

E_x (MeV)	J^{π}	Γ_α/Γ_p this work	Γ_α/Γ_p $S(\alpha,\gamma)/S(p,\gamma)$ [a)]	Γ_α [b)] (eV)	Γ_p (eV)	Γ_γ [c)] (eV)	θ_α^2 [d)] (%)	θ_p^2 [d)] (%)
11.52	2^+			≥ 0.01		≥ 0.01	≥ 0.8	
11.66	2^+			≥ 0.03		≥ 0.03	≥ 0.6	
11.93	$2^+,3^-,4^+$							
12.07	2^+	0.68 ± 0.30	0.84	0.48	0.71	0.17	0.34	0.17
12.29	2^+	0.065 ± 0.010	0.082	1.3	20	0.24	0.25	0.25
12.44	2^+	9.7 ± 2.3	5.3	22	2.2	0.41	1.9	0.0074
12.55	4^+	≥ 1	2.1	0.90	0.43	0.12	0.95	0.026
12.58	2^+ (T=1)	≤ 0.1			≥ 0.5	≥ 0.5		≥ 0.0007
12.73	2^+	0.79 ± 0.24	4.1	340	430	0.31	7.7	0.30
12.90	2^+	0.31 ± 0.10	0.65	60[e)]	190[e)]	0.97	0.69	0.065
13.09	4^+	≥ 0.2	5.6	51	9	0.12	4.8	0.035

a) $S(x,y) = (2J+1)\Gamma_x\Gamma_y/\Gamma$, $S(\alpha,\gamma)$ ref. 46, $S(p,\gamma)$ ref. 47 (corrected by a new calibration value)

b) $(2J+1)\Gamma_\alpha = S(\alpha,\gamma) + S(p,\alpha_0)(1+\Gamma_\alpha/\Gamma_p)$, $S(p,\alpha_0)$ ref. 39

c) $(2J+1)\Gamma_\gamma = S(p,\gamma)[1+\Gamma_\alpha/\Gamma_p + S(\alpha,\gamma)/S(p,\alpha_0)]$

d) $\gamma_w^2(\alpha) = 0.54$ MeV, $\gamma_w^2(p) = 2.4$ MeV

e) Ref. 50 $\Gamma = 250$ eV

for the 12.44 MeV level, respectively. The total widths of 22 eV and 25 eV are obtained by summing up the calculated partial widths in agreement with blocking measurements. For the 12.73 MeV level Γ = 770 eV is slightly higher than the values 660 ± 30 eV[50], 600 ± 60 eV[48] and 760 ± 170 eV[47] deduced from (p, p_0), (p, α_0) and (α,γ) resonance studies, respectively.

The penetrabilities given in table 9 relate to the lowest possible ℓ value and the reduced widths were determined using the Wigner width of 2.4 MeV for protons and 0.54 MeV for α particles. The reduced α widths are on an average 1 % of the Wigner limit while the reduced proton widths are less than 0.3 % of the corresponding limit.

4.4. Decay of ^{32}Cl

Targets containing natural sulphur (^{32}S 95.0 %) were used for the production of ^{32}Cl. Equal amounts of sulphur and polystyrene were dissolved in carbon disulphide. After evaporation of carbon disulphide homogeneous 2 mg/cm^2 thick foils were obtained.

A delayed particle spectrum measured with the 100 μm detector is shown in fig. 11. When the same experiment was repeated with the 13.9 μm detector 11 of the particle groups were confirmed to be due to α particles and 6 groups due to protons. In a previous study Steigerwalt et al.[6] observed in the decay of ^{32}Cl three proton groups and two α groups, which corresponds to the strongest groups in our spectra.

The energy calibration was carried out using the well-known level energies separately for protons and α particles. The deduced energies and intensities of the particle transitions are given in table 10. The binding energies used in the calibration were B_p = 8864.7 ± 0.5 keV and

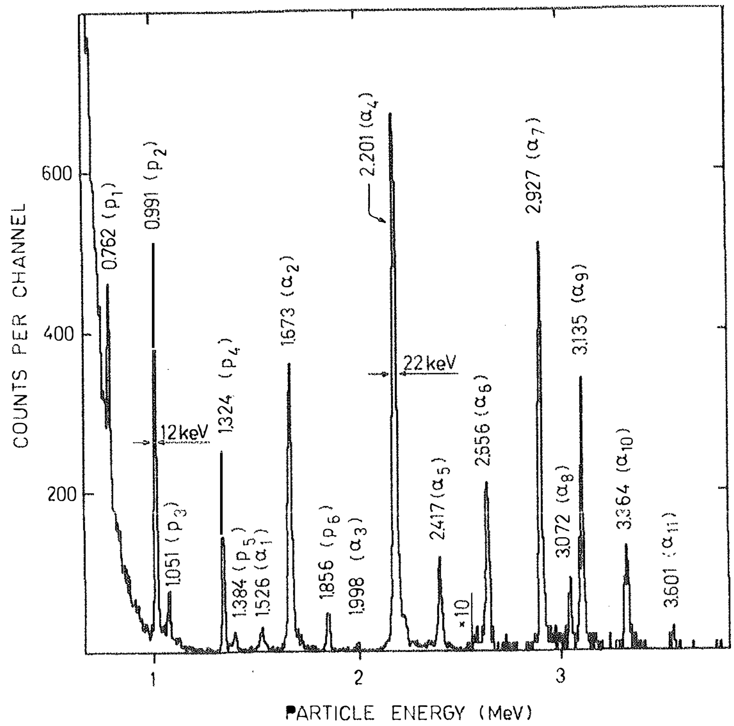

Fig. 11. Delayed particle spectrum of ^{32}Cl measured with the 100 µm detector. The collecting and measuring period was 600 ms and the integrated beam current 80 mC.

B_α = 6948.9 ± 0.5 keV[39]. The log ft values were calculated using a value Q_{EC} = 12687 ± 8 keV and a half-life of 298 ± 2 ms for ^{32}Cl[39]. Radiation widths were taken to be negligible with respect to particle widths. That this should be a good approximation for excitations over 9.5 MeV is supported by the partial widths given in table 11.

The observed delayed particle transitions can be assigned to the known energy levels in ^{32}S without introducing more than two additional levels. Allowed β-transitions from the ground state of ^{32}Cl ($J^\pi = 1^+$) populate levels which have $J^\pi = 0^+$, 1^+ and 2^+. Observed proton transitions to the ground state of ^{31}P ($J^{\pi} = 1/2^+$) originate from 1^+ and 2^+ levels. Alpha decay to the ground state of ^{28}Si ($J^{\pi} = 0^+$) is expected from 0^+ and 2^+ levels, but not from 1^+ levels because of parity forbiddenness.

Seven of the observed α transitions do originate from 2^+ levels and one from a 0^+ level. The levels at 9.89 and 9.95 MeV have previous assignments $J^{\pi} = (1, 2)$ and 1, respectively. Beta decay selection rules indicate even parity for both levels. The 2.00 MeV α transition apparently follows a forbidden β transition to the 1^- level at 9.24 MeV as indicated by the high log ft value.

The observed log ft values are compared in table 10 with the shell-model predictions in the compilation of Brown and Wildenthal[11]. They predict strong β transitions to T = 1 states at 9.77, 10.02 and 10.75 MeV. These are connected to the observed levels at 9.65, 9.89 and 10.78 MeV on the basis of the good agreement between the calculated and experimental log ft values. These are also good candidates for T = 1 states because neither α emission nor α pickup has been observed. The three levels are proposed to correspond to 2^+ states at 2.66, 3.88 MeV and a 1^+ state at 2.74 MeV in ^{32}P. Because the T = 1 analog state of the ^{32}P ground state is at 7.00 MeV in ^{32}S[39], the corresponding analog states should be at excitation energies of about 9.66, 10.88 and 9.74 MeV. Previously the analog of the 2.66 MeV 2^+ state has been assigned[39] to the 9.65 MeV level in agreement with the present interpretation, but the 2.74 MeV 1^+ state has been though to be the analog state of a 9.66 MeV $J^{\pi} = 1$ level[39].

Brown and Wildenthal have predicted four additional β transitions leading to T = 1 states at 10.38 (2^+), 10.61 (1^+), 10.67 (0^+) and 10.96 MeV (1^+) with log ft values 6.78, 6.67, 5.03 and 5.35, respectively. These high log ft values indicate weak β branchings, and so the particle emission of the corresponding levels was not observed in this work. Only two $J^{\pi} = 2^+$,

Table 10. Summary of delayed particle emission of ^{32}Cl

	particle energy (keV)	E_x in ^{32}S (keV) this work	previous[a]	$J^\pi;T$[a]	I_ν ($\times 10^{-6}$)	log ft_{exp}	E_x^{calc}[b] (keV)	$J^\pi;T$[b]	log ft_{calc}[b]
p_1	762±3	9651	9650.5±0.7	$2^+;1$	52 ± 8	≤5.5±0.1	9770	$2^+;1$	4.74
p_2	991±1[c]	9888	9887.9±0.8	$1^+,2^+;0+(1)$[c]	113 ±17	4.9±0.1	10020	$1^+;1$	4.93
p_3	1051±3	9950	9950.1±0.8	$1^+;0$[c]	19 ± 4	5.7±0.1	9780	$1^+;0$	5.85
p_4	1324±1[c]	10232	10231.7±0.8	$1^+;0$	52 ± 8	4.9±0.1	10320	$1^+;0$	4.84
p_5	1384±3	10293	10293.5±1.6	$2^+;0$	7.8± 2	5.1±0.1			
p_6	1856±3	10781	10779.5±1.1	$2^+;(1)$[c]	16 ± 3	4.5±0.1	10750	$2^+;1$	5.15
α_1	1526±5	8693	8690 ±2	$2^+;0$	11 ± 2	≤6.9±0.1	8370	$2^+;0$	7.61
α_2	1673±2[c]	8861	8861 ±2	$2^+;0$	146 ±20	≤5.7±0.1	8700	$2^+;0$	5.50
α_3	1998±8	9232	9236 ±2	$1^-;0$	2 ± 1	≤7.3±0.2			
α_4	2201±2[c]	9464	9464.1±1.1	$2^+;0$	300 ±42	4.9±0.1			
α_5	2417±3	9711	9711.5±0.7	$2^+;0$	40 ± 7	5.6±0.1			
α_6	2656±4	9984	9983.4±0.8	$0^+;0$	6.9± 2	6.0±0.1			
α_7	2927±2[c]	10294	10293.5±1.6	$2^+;0$	17 ± 3	5.1±0.1			
α_8	3072±5	10460		$0^+,2^+;0$[c]	2.4± 1	5.9±0.2			
α_9	3135±5	10532	10533 ±4	$2^+;0$	8.4± 2	5.3±0.1			
α_{10}	3364±2[c]	10793	10792.9±1.1	$2^+;0$	5.1± 1	5.0±0.1			
α_{11}	3601±5	11064		$0^+,2\ ;0$[c]	0.6± 0.3	5.5±0.2			

a) Ref. 39, b) Ref. 11, c) Partly or totally from this work

$T = 0$ levels, one at 8.37 and the other at 8.70 MeV, have been predicted by the shell model. These are associated with the 8.69 and 8.86 MeV states, because these are the only known 2^+ levels between 8 and 9 MeV. The truncation of the sd-shell space possibly causes the lack of predictions for β transitions to 2^+ states at higher excitations.

The partial width ratios obtained from the delayed particle spectra and from the (p,γ) and (α,γ) resonance yields are shown in table 11. From the (α,γ) and (p,γ) strengths measured by Rogers et al.[55] and Coetzee et al.[56], respectively, the partial width ratios can be determined for the 9.46 and 9.71 MeV states. Coetzee et al. normalized their results to a value of 0.52 eV for the E_p = 642 keV resonance, which was later measured[49] to have a strength of 0.24 ± 0.04 eV. Taking into account this new value the partial width ratios Γ_α/Γ_p of 26 ± 13 and 4.7 ± 2.4 are obtained for the two levels. The former differs considerably from the upper limit $\Gamma_\alpha/\Gamma_p \gtrsim 60$ determined from the delayed particle spectra, while the latter is not in conflict with the observed upper limit $\Gamma_\alpha/\Gamma_p \gtrsim 2$. However, the strengths from the (p,γ) study of O'Brien et al.[57] result in Γ_α/Γ_p = 120 ± 80 and 10 ± 4 in better agreement with our values. The proton group at 1.38 MeV and the α-particle group at 2.93 MeV were assigned to the decay of the same level at 10.29 MeV, because no other suitable levels at about 10.3 MeV are available according to resonance reaction data[39].

The partial widths are given in table 11 for the levels whose (p, α_0) strengths are known. Reduced widths do not indicate any level with strong α-cluster composition. However, the reduced α widths are in all cases notably higher than the corresponding proton widths.

Table 11. Properties of some ^{32}S levels decaying by delayed particle emission

E_x (MeV)	J^π	Γ_α/Γ_p this work	Γ_α/Γ_p $S(\alpha,\gamma)/S(p,\gamma)$ a)	Γ_α a) (eV)	Γ_p (eV)	Γ_γ a) (eV)	θ_α^2 b) (%)	θ_p^2 b) (%)
9.46	2^+	≥ 60	120	2.6	0.022	0.15	1.5	0.23
9.71	2^+	≥ 2.7	10	12	1.2	0.13	1.9	0.58
9.98	0^+	≥ 2.3		≥ 80	≥ 35	≥ 2.2	≥ 1	≤ 0.07
10.23	1^+				25 ± 10 c)	0.17		0.016
10.29	2^+	2.2 ± 0.5		40	18	0.12	0.55	0.19
10.53	2^+	≥ 4		≥ 24	≤ 6	≥ 0.01	≥ 0.2	≤ 0.03

a) $S(\alpha,\gamma)$ ref. 55, $S(p,\gamma)$ ref. 57, $S(p,\alpha_0)$ ref. 39

b) $\gamma_w^2(\alpha) = 0.50$ MeV, $\gamma_w^2(p) = 2.2$ MeV

c) Ref. 58

4.5. Decay of ^{36}K

The precursor nuclide ^{36}K was produced by the (p,n) reaction from ^{36}Ar. Because the isotopic abundance of ^{36}Ar in natural argon is only 0.34 %, enrichment of ^{36}Ar is necessary in order to have a sufficient yield of ^{36}K. The electromagnetic separator of the Helsinki University was employed in the preparation of ^{36}Ar targets. Argon gas enriched in ^{36}Ar (50 %) was fed to the ion source and ^{36}Ar ions were implanted into a thin aluminium foil near to saturation. Then a layer of about 70 nm of aluminium was evaporated onto the foil in a separate chamber. The implantation-evaporation cycle was repeated five times so that the layers had an approximate overall depth of 350 nm. The target composition was analyzed by means of alpha particle backscattering techniques. The thickness of the implanted layer was measured[59)] to be 110 $\mu g/cm^2$ of which about 19 $\mu g/cm^2$ consisted of ^{36}Ar. Using Northcliffe's tables[60)] the recoil range of ^{36}K ions was estimated to be 120 $\mu g/cm^2$ in the composite implanted layer. In the experiments the ^{36}Ar targets were irradiated with 20 MeV protons of 1 - 2 μA beam current. The total integrated beam current was about 400 mC. An analysis made afterwards showed that neither the spatial distribution nor the quantity of ^{36}Ar had noticeably changed during the irradiation.

Delayed particle spectra of ^{36}K measured with the 26 μm and 100 μm detectors are shown in figs. 12 and 13. The inset in fig. 13 displays the spectrum in the energy range 1.0 - 2.5 MeV. The spectrum was measured by a second 100 μm detector placed adjacent to the first 100 μm detector. In the second detector the β continuum extended only up to 1.3 MeV, because the spectrum was measured one 500 ms period later. All the particle groups measured with these adjacent detectors show up in the same proportion, which indicates that all the groups have the same half-life. The most prominent

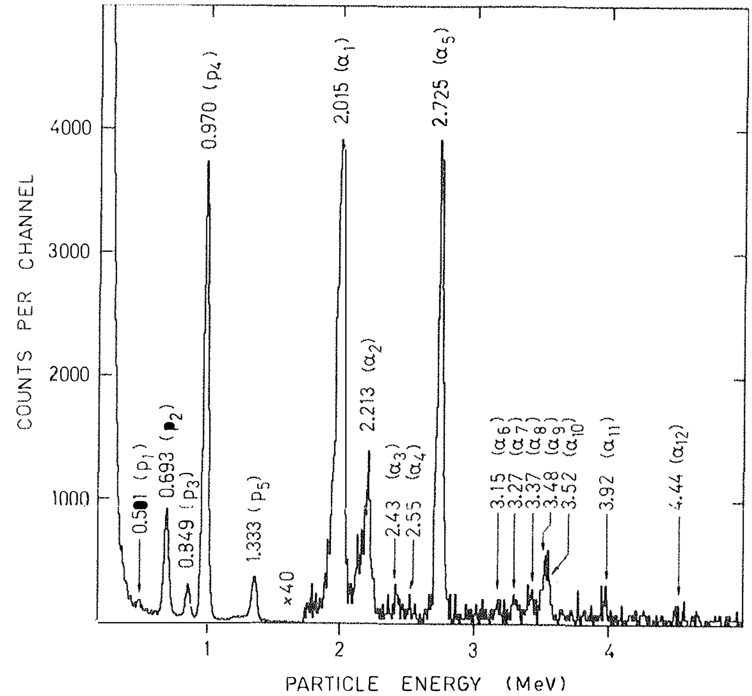

Fig. 12. Delayed particle spectrum of ^{36}K measured with the 26 μm detector. The collecting and measuring period was 500 ms and the integrated beam current 130 mC.

proton and α-particle groups were measured to decay with half-lives of 360 ± 40 ms in agreement with the known half-life of ^{36}K. The particles were identified as protons or α particles by comparison of the spectra displayed in figs. 12 and 13 and by absorption measurements. It was shown[59] by the absoprtion technique that the middle one of the three very close-lying particle groups at about 2 MeV is due to α particles and the other two are due to protons.

Ewan et al.[10] have studied the delayed particle emission of ^{36}K using a spallation reaction and a mass separator. They assign three proton groups

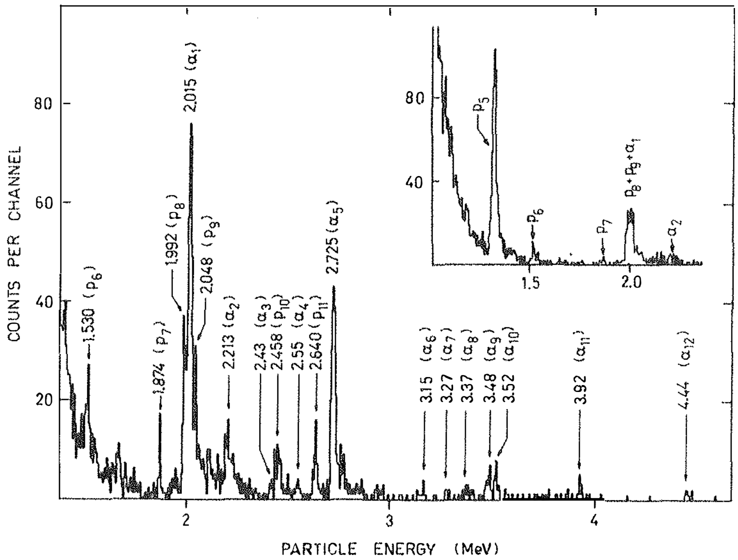

Fig. 13. Delayed particle spectrum of ^{36}K measured with the 100 μm detector. The inset shows a part of a spectrum measured one 500 ms period later with a second 100 μm detector.

and four α-particle groups to the decay of ^{36}K. Their experimental results are generally in good agreement with this study, but the interpretation of the data is somewhat different. The complex group at 2 MeV is suggested by Ewan et al. to be a sum of two α-particle groups and the 0.85 MeV proton group is assumed to be due to partial energy loss of the 1.33 MeV protons in the 20 μm detector.

The energy calibration of the particle spectra was done using the delayed particles associated with the decay of ^{32}Cl. The decay properties of ^{32}Cl were also used to determine the relative particle and γ-ray efficiencies of the detector configuration used for absolute branching ratio measurement. In the calculation of level energies and log ft values, binding energies B_p = 8506.6 ± 0.3 keV and B_α = 6641.1 ± 0.6 keV were used for ^{36}Ar and the values Q_{EC} = 12805 ± 8 keV and $T_{1/2}$ = 342 ± 2 ms for ^{36}K[39]. The results of the delayed particle emission studies are shown in table 12. These are compared with data from resonance reaction studies[39] and shell-model calculations[11]. All the predicted levels with E_x > 8.7 MeV are included in this table. The main argument linking a particle group with a certain resonance level is energy compatibility. Because the observed (p,γ) resonance level density of ^{36}Ar is about 60/MeV at an excitation energy of 10 MeV, the energy compatibility alone is not always sufficient for a unique assignment. Additional constraints on the selection of the resonance level are set by the measured upper limit of the log ft value or by the ratio Γ_α/Γ_p. In the decay of ^{36}K ($J^\pi = 2^+$) allowed transitions populate 1^+, 2^+ or 3^+ states in ^{36}Ar. The proposed spin and parity assignments for levels observed in this study are given in table 12.

All the observed proton and α-particle groups have been assigned to transitions leading to the ground state. The proton groups up to 2 MeV match well the (p,γ) resonance states and the energies are compatible with proton emission leading to the ground state of ^{35}Cl ($J^\pi = 3/2^+$). In contrast, the energies do not agree with the energies of (p, p_1) resonances as given by Johnson et al.[61] except possibly for the 693 keV group, the energy of which is only 3 keV above the p_1 proton energy of the 1984 keV proton resonance. The proton group observed at 2048 keV is clearly associated with an allowed β transition. The close-lying proton resonance at 10615 keV has been assigned $J^\pi = 4^-$ by γ-ray angular distribution measurements[62]. An overlapping resonance at 10616 keV was observed in a (p, α_0) reaction study[63] and assigned $J^\pi = (4^+, 5^-, 6^+)$. Because the present result is not compatible with either of the two levels, a third level with $J^\pi = 1^+$, 2^+ or 3^+ may be involved. The 11027 keV 3^+ level has been assigned to have T = 1 by Erne[64]. The calculated log ft value of

Table 12. Summary of delayed particle emission of ^{36}K

	particle energy (keV)	E_x in ^{36}Ar (keV) this work	previous$^{a)}$	$J^{\pi};T^{a)}$	I_{ν} ($\times 10^{-6}$)	log ft	$E_x^{calc\,b)}$	$J^{\pi};T^{b)}$	log ft_{calc} $^{b)}$
p_1	501±10	9022	9024.9±0.7	2 ;(1)	3.5± 1.2	≤ 7.3±0.2	9290	$2^+;1$	5.46
p_2	693± 5	9219	9219.9±1.1	$1^+;(1)$	75 ±22	4.5±0.2$^{c)}$	9700	$1^+,1$	4.57
p_3	849± 5	9380	9379.6±1.3	$2^+,3^{+g)};(1)$	19 ± 6	≤ 6.3±0.1	9330	$3^+;1$	4.28
p_4	970± 5	9504	9502.4±0.6	$2^+,3^+$	330 ±90	4.1±0.1$^{d)}$	9580	$3^+;0$	4.25
p_5	1333± 5	9878	9878.2±0.6	$2^+,3^+$	35 ±10	≤ 5.6±0.1	9210	$3^+;0$	5.26
			9982.9±0.6	$1^+,(2^+);1$	≤3	≥ 6.5	10270	$1^+;1$	6.35
p_6	1530±10	10080	10076.4±0.6	$1^- -3$	3.0± 1.2	6.5±0.2			
p_7	1874±10	10434	10439 ±2	$2^+;0$	1.1± 0.5	6.3±0.2$^{e)}$	10650	$2^+;0$	6.01
p_8	1992±10	10556	10558 ±2	$2^+;0$	4.8± 1.9	5.6±0.2$^{f)}$			
p_9	2048±10	10613		$1^+-3^{+g)}$	4.7± 1.8	5.6±0.2	11220	$3^+;0$	5.77
p_{10}	2458±10	11035	11027 ±2 11046 ±2	$3^+;1$	2.9± 1.2	5.1±0.2	10280 10880	$3^+;1$ $1^+;0$	8.99 5.06
p_{11}	2640±10	11222	11215 ±2 11230 ±2	$1^+-3^{+g)}$	2.0± 0.9	4.9±0.2	11110 11250 11830	$2^+;1$ $1^+;0$ $3^+;1$	5.53 5.23 5.32

α_1	2015± 5	8908	8911 ±5	$2^+;0$	15 ±5	$\leq$ 6.8±0.2	8770	$2^+;0$	5.41
α_2	2213±10	9132	9132.1±0.7 9144.5±0.7	3^- $(2^+,3^-)$	4.4±1.8	$\leq$ 7.1±0.2			
α_3	2430±15	9375	9365.6±0.8 9373.7±1.3 9379.6±1.3	$1^-;0$ (1^--3) $2^+,3^+;(1)$	0.3±0.2	$\leq$ 8.1±0.3			
α_4	2553±15	9513	9494.0±1.2 9502.4±0.6 9509.2±0.7	 $2^+,3^+;0$ (2^+-4^+)	0.2±0.2	$\leq$ 8.2±0.3			
α_5	2725± 5	9707	9702.8±1.4	$1^-,2^+;0$	10 ±4	$\leq$ 6.4±0.2	9500	$2^+;0$	5.32
α_6	3146±15	10180	10173.0±0.6	$(1^-,2^+);0$[g]	0.2±0.2	7.5±0.3			
α_7	3271±15	10321	10319.1±1.5	$2^+;0$	0.3±0.2	7.2±0.3	10690	$2^+;0$	7.57
α_8	3375±15	10438	10439 ±2	$2^+;0$	0.6±0.3	6.3±0.3[e]	10650	$2^+;0$	6.01
α_9	3479±15	10555	10558 ±2	$2^+;0$	1.1±0.5	5.6±0.3[f]			
α_{10}	3516±15	10597	11593 ±2	$2^+;0$	0.8±0.4	6.4±0.3			
α_{11}	3922±15	11053	11050 ±3	$2^+;0$[g]	0.4±0.2	5.9±0.3	10980	$2^+;0$	4.73
α_{12}	4443±20	11639		$2^+;0$[g]	0.4±0.2	4.9±0.3	11810 12190 12340	$2^+;0$ $2^+;0$ $2^+;0$	4.76 4.82 6.32

a) Ref. 39

b) Ref. 11

c) Γ_p/Γ = 0.048, see table 13

d) Γ_p/Γ = 0.13 , see table 13

e) Γ_α/Γ_p = 0.55, see table 13

f) Γ_α/Γ_p = 0.23, see table 13

g) Partly or totally from this work

the 10930 $J^{\pi} = 3^{+}$, T = 1 state is 8.99 and thus this level should not be seen in this work. It is possible that the 2458 keV proton group is associated with another (p,γ) resonance at 11046 observed by Johnson et al.[61]. The identification of observed levels with calculated ones at above 11 MeV of excitation is difficult because of the high level density and because spins and parities are known only in very few cases.

The very weak α-particle groups at 2430 and 2553 keV may be associated with the levels at 9366 and 9494 keV observed in the (p,α_0) reaction[63] or with the (p,γ) resonance levels[61] at 9374 and 9509 keV. The possibility that these groups are associated with the 9380 and 9502 keV levels cannot be completely excluded. However, as discussed later, the 9380 keV level has been thought to have a T = 1 character. Hence α decay from this level would be isospin forbidden. Shell-model calculations indicate that the proton emitting levels at 9380 and 9502 keV have $J^{\pi} = 3^{+}$ and thus the α decay would also be parity forbidden. Therefore, it is concluded that the levels associated with proton and α-particle emission are not the same.

The 2725 keV α-particle group was assigned to the decay of the (p,α_0) resonance level at 9703 keV. The angular distribution measurements restrict the possible J^{π} values of this level to 0^{+}, 1^{-} and 2^{+}. Since the observed value of log ft = 6.4 excludes the $J^{\pi} = 0^{+}$ assignment, this state cannot be identified with the 0^{+}, T = 1 level at $E_x = 9.70 \pm 0.03$ MeV observed in the $^{38}Ar(p,t)^{36}Ar$ reaction[65]. The α-particle groups with $E_{\alpha} > 3.2$ MeV are all associated with $J^{\pi} = 2^{+}$ levels, either because they are connected with observed (p,α_0) resonance levels or because β transitions preceding the α-particle emission are allowed.

When the delayed particle data are combined with the results of β-delayed γ-ray study of Fritts[66], both protons and γ rays are observed in the decay of the 9219 and 9504 keV levels. Using the γ branchings of

$1.5 \cdot 10^{-3}$ and $2.3 \cdot 10^{-3}$ [66] and the measured proton intensities the proton width can be calculated to be $\Gamma_p/\Gamma = 0.048$ for the 9.22 MeV level and $\Gamma_p/\Gamma = 0.13$ for the 9.50 MeV level. It has been assumed that the α-decay width associated with the third open channel is negligible. This assumption is justified by the measured particle spectra, which indicate the α width to be very small compared with proton width (see table 13). The γ branchings have been taken into account in the log ft calculations. The log ft values predicted by the shell model for the ($J^{\pi} = 1^+$; T = 1) level at 9.70 MeV and for the (3^+ ; 0) level at 9.58 MeV agree well with the experimental values for the levels mentioned above. The calculated ft values for the 9.29 MeV (2^+ ; 1) and the 9.33 MeV (3^+ ; 1) levels are two orders of magnitude lower than those observed for the 9.02 MeV (2 ; 1) and 9.38 MeV (2^+, 3^+ ; 1) levels. The γ branchings from these levels have not been observed in the study of Fritts, but the (p,γ) strengths indicate that these levels have relatively high γ widths.

The first three states in table 12 and the 9.98 MeV 1^+ (2^+) state have been assigned T = 1 and they are considered to be analogs of the 2.49 MeV 2^+, 2.68 MeV $1^+(2^+)$, 2.86 MeV $(2, 3)^+$ and 3.47 MeV $(1, 2)^+$ states of ^{36}Cl. The 9.98 MeV level was not observed experimentally but the estimated upper limit of the log ft value is in reasonable agreement with the calculated value. The mutual compatibility between calculated and observed levels is good, if the α-particle emitting levels between 9.1 and 9.6 MeV and the level at 10.18 MeV are excluded, because they are possibly populated by forbidden β transitions. Also the calculated β-transition strengths agree with the observed values within experimental uncertainty. However, the strong β transition with log ft = 4.73 predicted to a 2^+ level at 10.98 MeV is not observed and it is likely that its strength is distributed over many levels. It is also possible that some of the β strength to levels above

10 MeV is spread over the high energy part of the delayed particle spectrum as seen from fig. 12.

The partial widths Γ_p and Γ_γ for the 9.22 and 9.50 MeV levels given in table 13 were derived from the (p,γ) resonance strengths and from the Γ_p/Γ ratio. The (p,γ) strengths measured by Johnson et al. were reduced by 12 % due to a new calibration value[49)] for an E_p = 860 keV resonance. The partial γ width for the 9.22 MeV level is an order of magnitude higher than those for T = 0 levels (see e.g. table 9) indicating a T = 1 nature.

The partial widths Γ_α and Γ_p were determined from the (p, α_0) resonance strengths and from the partial width ratios Γ_α/Γ_p obtained from the delayed particle spectra. The proton widths in table 13 are of the same magnitude as the α widths. Because the penetrabilities are much higher for protons, the reduced proton widths are clearly smaller than the reduced γ widths. It is remarkable that only one of the observed α-particle groups, that at 2015 keV, has been seen in (α,γ) resonance studies and only two at 2213 and 3146 keV have been seen in (p,γ) studies. All the other levels have been seen only in the (p, α_0) reaction.

Table 13. Properties of some ^{36}Ar levels decaying by delayed particle emission

E_x (MeV)	J^π	Γ_α/Γ_p	Γ_p/Γ a)	Γ_α b) (eV)	Γ_p (eV)	Γ_γ (eV)	θ^2_α c) (%)	θ^2_p c) (%)
9.22	1^+ (T=1)	≤ 0.003	0.048		0.3 d)	5 d)		0.07
9.50	$2^+, 3^+$	≤ 0.0006	0.13		$0.4/\bar{J}$ d)	$3/\bar{J}$ d)		0.0010 (2^+) 0.021 (3^+)
10.32	2^+	≥ 0.4		≥ 20	≤ 60	≥ 0.1	≥ 0.5	≤ 0.02
10.44	2^+	0.55 ± 0.45		77	140		1.2	0.033
10.56	2^+	0.23 ± 0.08		34	150		0.37	0.027
10.59	2^+	≥ 0.6		≥ 70	≤ 120		≥ 0.7	≤ 0.02
11.05	2^+	≥ 0.5		≥ 150	≤ 300		≥ 0.4	≤ 0.02

a) See text

b) $(2J+1)\Gamma_\alpha \approx S(p,\alpha_0)(1+\Gamma_\alpha/\Gamma_p)$; $S(p,\alpha_0)$ ref. 63

c) $\gamma^2_w(\alpha) = 0.46$ MeV, $\gamma^2_w(p) = 2.1$ MeV

d) $S(p,\gamma) = \bar{J}\,\Gamma_p\Gamma_\gamma/\Gamma$; $S(p,\gamma)$ ref. 61; $\bar{J} = 2J+1$

4.6. Decay of ^{40}Sc

Delayed particticle spectra of ^{40}Sc measured with the 100 μm and 31.1 μm detectors are displayed in figs. 14 and 15. These were obtained by bombarding natural calcium (^{40}Ca 96.9 %) by 20 MeV protons. All the peaks below 2.5 MeV except for those at 1.98 and 2.09 MeV were found to be due to protons by comparing the two spectra and by energy degradation measurements[67]. The half-lives of the 1.98 and 2.09 MeV groups were measured to be 2.2 ± 0.8 s and 170 ± 30 ms, respectively. The energy and the half-life of the former group are consistent with the decay of ^{24}Al induced by Mg impurities, while the half-life of the latter group is consistent with the known half-life of 182.3 ± 0.7 ms of ^{40}Sc. The average half-lives of the proton and α-particle groups were measured to be 182.4 ± 1.8 and 183 ± 7 ms, respectively.

The energy calibration was done separately for protons and α particles. The well-known proton resonances at 9602 ± 1, 10212 ± 2 and 11218 ± 3 keV were used for proton energy calibration[39,68]. The most prominent β-delayed α-particle groups of ^{20}Na were used for the α-particle energy calibration. Measured energies and intensities of proton transitions are given in table 14 and those for α particles in table 15. Energies of excited states in ^{40}Ca were calculated by using the binding energies B_p = 8329.7 ± 0.5 keV and B_α = 7040.5 ± 0.9 keV[39]. In the calculation of log ft values the total decay energy of 14320 ± 4 keV[39] was used for ^{40}Sc. In the cases where proton and α-particle emission were associated with the same level both branchings were taken into account. The given log ft values must be considered as upper limits because no information of γ branchings is available.

Allowed β transitions from the 4^- ground state of ^{40}Sc can populate 3^-, 4^- and 5^- states in ^{40}Ca. Out of these only 3^- states can decay to the $3/2^+$

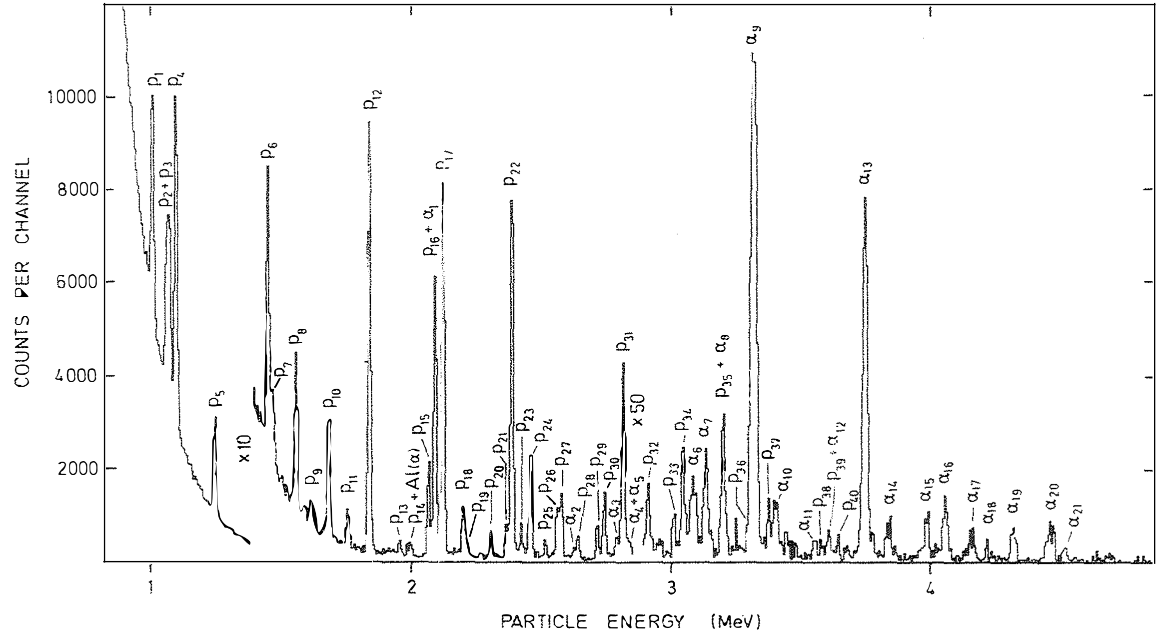

Fig. 14. Delayed particle spectrum of ^{40}Sc measured with the 100 μm detector. The collecting and measuring period was 600 ms and the integrated beam current 60 mc.

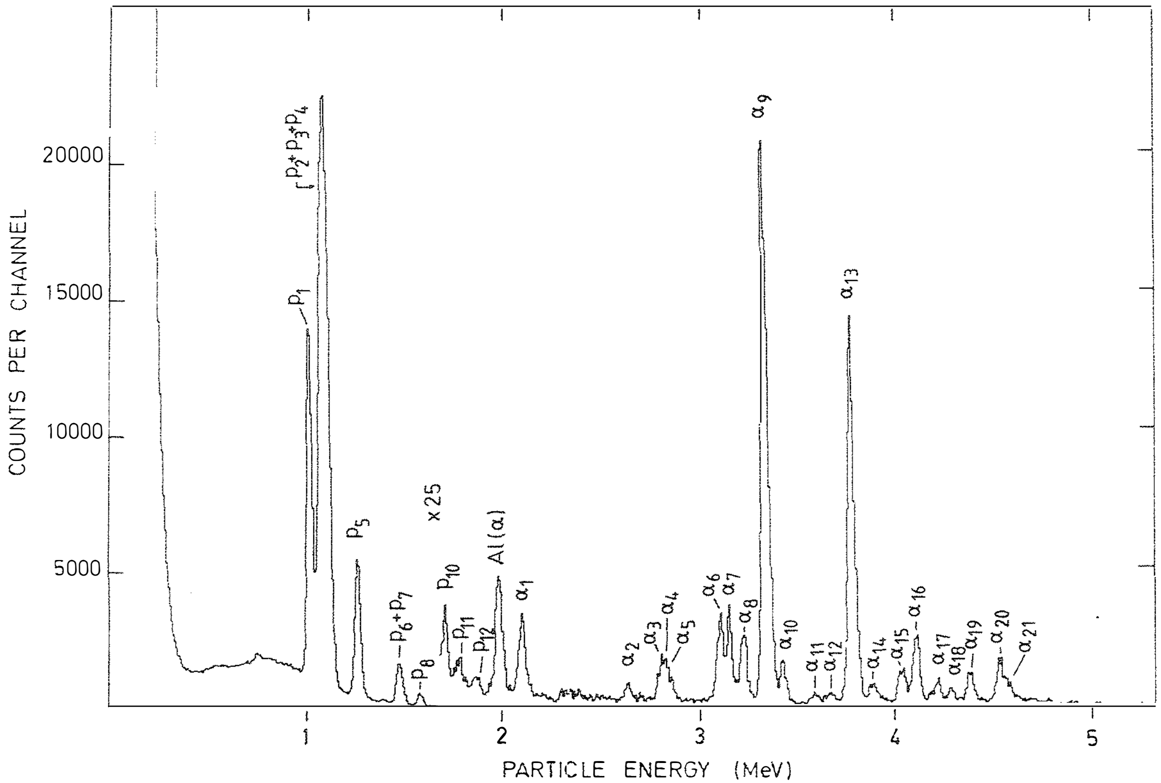

Fig. 15. Delayed particle spectrum of ^{40}Sc measured with the 31.1 μm detector. The collecting and measuring period was 500 ms and the integrated beam current 130 mc.

ground state of ^{39}K by emission of $\ell = 1$ protons. Because the penetrability for $\ell = 3$ protons is $\leq 10^{-5}$ below the 9.5 MeV excitation energy compared to a penetrability of $\leq 10^{-3}$ for $\ell = 1$ protons, the 3^- assignment is more likely for these levels. The spin and parity assignments derived from our experiment are based on β-decay selection rules and in the case of α emission leading to the 0^+ ground state of ^{36}Ar the initial levels are further restricted to natural parity states.

Delayed proton emission in ^{40}Sc was first observed by Verall and Bell[8] and later studied by Sextro et al.[9]. In the former work 18 and in the latter 10 proton groups were assigned to ^{40}Sc. Because of the use of a particle telescope the energy resolution was not sufficient to resolve all individual transitions. The relative intensities of the major proton groups are in good agreement with our results, except for the appearance of a prominent 1.34 MeV group, which Sextro et al. have tentatively assigned to the decay of ^{40}Sc.

Most of the delayed proton transitions can be assigned to known energy levels in ^{40}Ca up to 10.5 MeV. At higher excitations the relatively high level density and lack of resonance data make comparisons difficult. For example, strong delayed proton transitions originating from the levels at 10472, 10505, 10777 and 10850 keV do not have corresponding levels observed in (p,γ), (p, p_0) or (p, α_0) resonance reactions. Levels at 10779 and 10851 keV were observed via the (p, α_0) reaction by de Meijer et al.[68], but they were uniquely assigned to have $J^\pi = 1^-$ and thus they cannot be populated in the β-decay of ^{40}Sc.

Table 14. Summary of delayed proton emission of ^{40}Sc

	Proton energy (keV)	E_x in ^{40}Ca (keV) This work	E_x in ^{40}Ca (keV) Previous	J^π; T	Proton branching ($\times 10^{-6}$)	log ft	
p_1	1006 ± 3	9361	9363 ± 1[b]	3^- [b,e]; 0	720 ± 110	5.4 ± 0.1	(p + α)
p_2	1060 ± 8	9417	9418 ± 1[b]	$3^-(4^-)$[b,e]; 1	440 ± 75	5.6 ± 0.2	
p_3	1071 ± 6	9428	9429 ± 1[b]	$3^-(4^-,5^-)$[e]	550 ± 95	5.5 ± 0.2	
p_4	1095 ± 3	9453	9454 ± 1[b]	3^- [b]; 0+1	1100 ± 170	5.2 ± 0.1	
p_5	1241 ± 3[a]	9602	9602 ± 1[b]	3^- [b]; 1	320 ± 50	5.6 ± 0.1	
p_6	1445 ± 4	9812	9810 ± 1[b]	$(3\text{-}5)^-$ [b]	88 ± 15	6.1 ± 0.1	
p_7	1463 ± 8	9830	9829 ± 1[b]	3-5[e]	26 ± 7	6.6 ± 0.1	
p_8	1552 ± 3	9921	9921 ± 1[b]	3-5[e]	50 ± 9	6.3 ± 0.1	
p_9	1609 ± 5	9980		3-5[e]	9.2 ± 5	7.0 ± 0.2	
p_{10}	1678 ± 4	10051	10051 ± 2[b]	4^- [b]; 1[e]	42 ± 9	6.3 ± 0.1	
p_{11}	1752 ± 4	10127	10129 ± 2[b]	$(3^-,4^+)$[b]; 0[e]	13 ± 4	6.7 ± 0.1	(p + α)
p_{12}	1835 ± 4[a]	10212	10212 ± 2[b]	$(3,4)^-$ [b]	139 ± 22	5.7 ± 0.1	
p_{13}	1953 ± 4	10333	10336 ± 2[b]	3^- [b,e]; 0	4.6 ± 2	7.1 ± 0.2	
p_{14}	1986 ± 8	10367	10366 ± 2[b]	3^- [b]; 0	3.0 ± 2	7.2 ± 0.3	

Table 14. cont.

p_{15}	2065 ± 4	10448	10448 ± 2[b]	3^- [b];0	28 ± 5	6.2 ± 0.1	
p_{16}	2089 ± 4	10472		$3^- - 5^-$ [e]	94 ± 14	5.7 ± 0.1	
p_{17}	2121 ± 4	10505		$3^- - 5^-$ [e];0	125 ± 19	5.5 ± 0.1	
p_{18}	2197 ± 5	10583		3-5[e]	17 ± 4	6.3 ± 0.1	
p_{19}	2211 ± 10	10597	10598 ± 2[c]	3^- [c,e];0	3.5 ± 2	6.5 ± 0.2	$(p + \alpha)$
p_{20}	2305 ± 5	10694		3-5[e]	7.6 ± 3	6.6 ± 0.2	
p_{21}	2365 ± 8	10755	10752 ± 3[c]	$(4^+,5^-)$[c];0	9.2 ± 3	6.5 ± 0.2	
p_{22}	2386 ± 5	10777		$3^- - 5^-$ [e]	128 ± 20	5.3 ± 0.1	
p_{23}	2423 ± 9	10815		3-5[e]	8.1 ± 3	6.5 ± 0.2	
p_{24}	2457 ± 5	10850		$3^- - 5^-$ [e]	38 ± 2	5.8 ± 0.1	
p_{25}	2516 ± 5	10910		3-5[e]	3.5 ± 2	6.8 ± 0.2	
p_{26}	2562 ± 8	10957	10956 ± 3[c]	3-5[e];0	20 ± 4	6.0 ± 0.1	
p_{27}	2578 ± 7	10974		3-5[e]	20 ± 4	6.0 ± 0.1	
p_{28}	2641 ± 7	11038		3-5[e]	6.9 ± 2	6.4 ± 0.1	
p_{29}	2716 ± 6	11115		3-5[e]	11 ± 3	6.1 ± 0.1	

Table 14. cont.

p_{30}	2743 ± 6	11143		3^--5^- [e]	23 ± 4	5.8 ± 0.1	
p_{31}	2816 ± 5[a]	11218	11218 ± 3[c]	3^- [c];1	68 ± 11	5.2 ± 0.1	
p_{32}	2912 ± 5	11316		3-5[e]	5.1 ± 2	6.3 ± 0.2	
p_{33}	3012 ± 7	11419	11418 ± 3[c]	4^+ [c];0	2.8 ± 2	6.4 ± 0.3	
p_{34}	3045 ± 9	11453	11449 ± 3[c]	3^--5^- [e];0	8.3 ± 2	5.9 ± 0.1	
p_{35}	3205 ± 10	11617	11622 ± 4[d]	3-5[e];0	2.4 ± 1	6.3 ± 0.2	
p_{36}	3308 ± 10	11723	11724 ± 4[d]	3^--5^- [e];0	7.3 ± 3	5.7 ± 0.2	
p_{37}	3376 ± 10	11792	11787 ± 4[d]	3-5[e];0	2.6 ± 2	6.0 ± 0.3	
p_{38}	3584 ± 10	12006	11993 ± 4[d]	3^- [d];0	1.0 ± 1	5.4 ± 0.2	$(p + \alpha)$
p_{39}	3613 ± 10	12035	12035 ± 4[d]	$(4^+,3^-)$[d];0	2.4 ± 1	5.8 ± 0.2	
p_{40}	3649 ± 10	12072	12068 ± 4[d]	3^- [d];0	1.2 ± 1	5.6 ± 0.3	$(p + \alpha)$

a) Used for calibration

b) Ref. 39

c) Ref. 68

d) Ref. 69

e) This work

Table 15. Summary of delayed alpha-particle emission of ^{40}Sc

	Alpha energy (keV)		E_x in ^{40}Ca (keV) This work	Previous	J^{π}; T	Alpha branching ($\times 10^{-6}$)	Γ_{α}/Γ_p	$\theta_{\alpha}^2/\theta_p^2$	log ft
α_1	2089 ±	6	9362	9363 ± 1[a)]	3^- [a,d)];0	8.8 ± 2	0.0119 ± 0.0005	190	5.4 ± 0.1
α_2	2620 ±	8	9952		$3^-,4^+,5^-$ [d)];0	1.6 ± 1	$\geq$ 0.5	$\geq$ 3000	7.7 ± 0.3
α_3	2780 ±	8	10129	10129 ± 2[a)]	$(3^-,4^+)$[a)];0	1.9 ± 1	0.14 ± 0.05	570	6.7 ± 0.1
α_4	2802 ±	8	10154		$3^-,4^+,5^-$ [d)];0	3.2 ± 1	$\geq$ 2	$\geq$ 7000	7.3 ± 0.2
α_5	2837 ±	8	10193		$3^-,4^+,5^-$ [d)];0	2.1 ± 1	$\geq$ 1	$\geq$ 3000	7.5 ± 0.2
α_6	3082 ±	7	10465		$3^-,4^+,5^-$ [d)];0	7.8 ± 2	$\geq$ 1	$\geq$ 1800	6.8 ± 0.1
α_7	3132 ±	7	10519		$3^-,4^+,5^-$ [d)];0	8.3 ± 2	$\geq$ 2	$\geq$ 3400	6.7 ± 0.1
α_8	3203 ±	7	10599	10598 ± 2[b)]	3^- [b,d)];0	6.9 ± 2	2.0 ± 0.7	2900	6.5 ± 0.1
α_9	3316 ±	5	10725		$3^-,5^-$ [d)];0	59 ± 12	$\geq$ 30	$\geq$33000	5.7 ± 0.1
α_{10}	3401 ±	7	10819		$3^-,4^+,5^-$ [d)];0	4.2 ± 2	$\geq$ 0.5	$\geq$ 470	7.7 ± 0.2
α_{11}	3552 ±	12	10987		$3^-,4^+,5^-$ [d)];0	1.1 ± 1	$\geq$ 0.2	$\geq$ 130	7.2 ± 0.4
α_{12}	3643 ±	12	11088	11092 ± 3[b)]	$4^+(3^-)$[b)];0	1.0 ± 1	$\geq$ 0.5	$\geq$ 250	7.1 ± 0.4
α_{13}	3748 ±	5	11205		$3^-,5^-$ [d)];0	38 ± 8	$\geq$ 6	$\geq$ 2500	5.5 ± 0.1

Table 15. cont.

α_{14}	3839 ± 7	11306		$3^-,4^+,5^-$ [d];0	2.4 ± 1	$\geq$ 1	$\geq$ 340	6.6 ± 0.2
α_{15}	3988 ± 7	11472	11468 ± 4[c]	$3^-,4^+,5^-$ [d];0	3.6 ± 1	$\geq$ 1	$\geq$ 250	6.2 ± 0.1
α_{16}	4058 ± 6	11549	11547 ± 4[c]	$3^-,5^-$ [d];0	6.6 ± 2	$\geq$ 6	$\geq$ 1300	5.9 ± 0.1
α_{17}	4160 ± 7	11663	11665 ± 4[c]	$3^-,4^+,5^-$ [d];0	2.3 ± 1	$\geq$ 2	$\geq$ 350	6.2 ± 0.2
α_{18}	4218 ± 7	11727	11729 ± 4[c]	$3^-,4^+,5^-$ [d];0	0.9 ± 1	$\geq$ 0.2	$\geq$ 30	6.6 ± 0.5
α_{19}	4320 ± 6	11841	11843 ± 4[c]	$3^-,5^-$ [c];0	2.8 ± 1	$\geq$ 0.7	$\geq$ 90	5.9 ± 0.2
α_{20}	4462 ± 7	11998	11993 ± 4[c]	3^- [c];0	5.0 ± 2	5 ± 2	500	5.4 ± 0.2
α_{21}	4519 ± 9	12062	12068 ± 4[c]	3^- [c];0	1.6 ± 1	1.3 ± 0.7	120	5.6 ± 0.3

a) Ref. 39

b) Ref. 68

c) Ref. 69

d) This work

Based on the barrier penetrability calculations alpha transitions to the first excited state in ^{36}Ar should be experimentally observable from states above 11.5 MeV excitations. However, the barrier penetrabilities for the ground state transitions are typically two orders of magnitude higher than those leading to the first excited state. Thus, the alpha groups leading to this state should have their associated ground state groups observable in the alpha spectrum and such peaks were not found. Moreover, an observable α transition with more than 3 MeV energy leading to the first excited state would imply prohibitively low log ft values. Nevertheless it is not completely excluded that some of the groups $\lesssim$ 3 MeV lead to the first excited state, but because of the lack of α_1 channel data all the alpha groups were assigned to the transitions leading to the ground state of ^{36}Ar.

The energies of the excited states deduced from the delayed alpha spectrum do not correspond very well with the levels obtained from the $(p\ ,\alpha_0)$ resonance work of de Meijer et al.[68]. For example, the two strongest transitions with 3317 and 3749 keV energies were not seen in this work at all. This would suggest strong collectivity or alpha-clustering associated with these levels because they are not strongly populated by a single proton induced reaction. The assignment of the levels above 11 MeV with those observed in a $(p\ ,\alpha_0)$ reaction study of Nakashima[69] is tentative because the resonance density is so high that several resonances can be assigned to each level. A recent inelastic α-particle scattering study on ^{40}Ca by van der Borg et al.[70] revealed a 3^- state at 9.34 MeV with a considerable α strength. They assign this state to the 9.363 MeV level, which supports the fixing of the 2.09 MeV delayed α-particle group to this level.

The ground state analog of ^{40}K is found[39] in ^{40}Ca at 7.66 MeV. Thus the 2.07 MeV 3^-, 2.29 MeV $(3, 4)^-$, 2.40 MeV 4^- and 3.87 MeV (3^-) states of ^{40}K should have analog states at about 9.73, 9.95, 10.06 and 11.53 MeV in ^{40}Ca. Good candidates [39] for the 2.07 MeV analog state are the 9.42, 9.45 or 9.60 MeV 3^- states, which exhibit T = 1 properties in the strength of their γ decay. All these levels have been observed in the present work and they emit only delayed protons. It is possible that the analog of the 2.07 MeV state is divided over these three levels. Suitable candidates for the analog of the 2.29 and 2.40 MeV levels are the 9.83 and 10.05 MeV states, which also decay[71] by a strong γ transition to bound T = 0 states. The ΔT = 0 γ transitions are inhibited in self-conjugate nuclei by isospin selection rules. Endt[72] has given a recommend upper limit of 0.03 Weisskopf units for isospin retarded M1 transitions. The 10.05 MeV 4^- state decays[71] by an M1 γ transition of 0.17 W.u. strength to a 7.12 MeV $J^\pi = 4^-$, T = 0 state, which clearly indicates T = 1 properties for this level. The 3^- level at 11218 keV is suggested[68] to be the T = 1 analog state of the 3.87 MeV (3^-) [73] state. Because α-emission is inhibited from T = 1 levels, all the α-particle emitting levels are assumed to have a T = 0 character or at least a notable T = 0 component.

Both proton and α-particle emission have been associated with the decay of five levels on the grounds of energy compatibility. Because the sensitivity of α-particle detection was about 10^{-6} the proton branchings in table 14 give directly the ratio Γ_p/Γ_α. In those cases where proton emission is not observed the lower limit for Γ_α/Γ_p as deduced from the background of the spectra are given in table 15. The reduced width ratios were also determined by calculating the barrier penetrabilities for the lowest possible ℓ value (i.e. assumed $J^\pi = 3^-$). These values express more clearly α-particle than single-particle properties for these states, especially for the 10.73

and 11.20 MeV levels.

The properties of some 3^- levels of ^{40}Ca are shown in table 16. The partial width ratios are from this work except for the 10.37 and 10.45 MeV levels for which these ratios were determined from (p, α_0) and (p, p_0) resonance yields. For the level at 9.45 MeV the proton width is determined from the (p, p_0) yield by assuming $\Gamma_p \approx \Gamma$. The reduced widths indicate a strong single-particle structure for the 9.45 and 10.37 MeV levels and a more collective structure for other levels.

The experimental β^+-decay strength is presented in fig. 16 in terms of reduced Gamow-Teller transition probabilities B' (GT) integrated over 250 keV intervals. The data for bound states are from ref. 30 and the data for unbound states are from our work. The reduced Fermi transition probability is assumed to be negligible except for the superallowed transition between the analog states. Raman et al.[12] have deduced the GT matrix element for this transition from the experimental log ft value and also by the shell model. From these results the values of $B'(GT)_{exp} = 0.67 \pm 0.16$ (partial log ft = 3.77) and $B'(GT)_{calc} = 0.952$ are obtained. As can be seen from fig. 16, β-decay strength to unbound states is mainly concentrated on two regions at 9.5 and 11 MeV.

By using the shell model description the dominant configuration of the ^{40}Sc ground state is expected to be $\pi f_{7/2} \nu d_{3/2}^{-1}$. This restricts the final configurations populated by allowed β decay to $f_{7/2}\, d_{3/2}^{-1}$, $f_{7/2}\, d_{5/2}^{-1}$ and $f_{5/2}\, d_{3/2}^{-1}$. The levels below 8 MeV have been shown[74] to arise from $f_{7/2}\, d_{3/2}^{-1}$ configurations. By using experimental single-particle energies from ^{39}K and ^{41}Ca the main amplitude of both the $f_{7/2}\, d_{5/2}^{-1}$ and the $f_{5/2}\, d_{3/2}^{-1}$ configurations can be estimated to be at 13.5 MeV in ^{40}Ca. The particle-hole model of Gillet and Sanderson[75] for the odd-parity states of ^{40}Ca indicates that $[f_{7/2}\, d_{5/2}^{-1}]^{3-}$ and $[f_{5/2}\, d_{3/2}^{-1}]^{3-}$ configurations have

Table 16. Properties of some ^{40}Ca levels decaying by delayed particle emission

E_x (MeV)	J^π	Γ_α/Γ_p	$S(p,\alpha_0)$ [a] (eV)	Γ_α (eV)	Γ_p (eV)	θ^2_α [b] (%)	θ^2_p [b] (%)
9.45	3^-	$\leq$0.001		$\leq$0.09	90 [d]	$\leq$65	4.3
10.13	3^-	0.14±0.05	7.9	1.3	9.3	8.4	0.015
10.37	3^-	0.000063 [a]	1.7	0.24	3800	0.42	2.7
10.45	3^-	0.0021 [a]	6.5	0.93	440	1.1	0.26
10.60	3^-	2.0±0.7	63	27	14	17	0.0058
11.99	3^-	5 ±2	400 [c]	340	69	2.1	0.0040
12.07	3^-	1.3±0.7	270 [c]	89	68	0.45	0.0037

a) Ref. 68

b) $\gamma^2_w(\alpha) = 0.43$, $\gamma^2_w(p) = 2.0$ MeV

c) Ref. 69

d) Ref. 68 , assumed $\Gamma_p \approx \Gamma$

a considerable amplitude at 11.66 MeV, which possibly explains the enhanced β strength at 11 MeV. However, between 9 and 10 MeV a very small amplitude for each of the earlier-mentioned configurations is predicted. Gerace and Green[76] used a mixture of shell model 1p - 1h states and 3p - 3h deformed states and they arrived[77] at similar results.

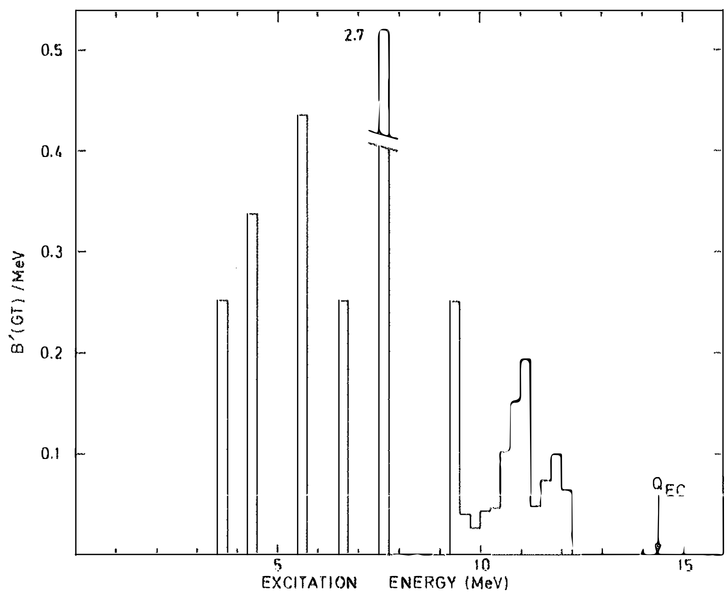

Fig. 16. Experimental β^+ strength of ^{40}Sc presented in terms of reduced β-transition probabilities B' (GT) as a function of excitation energy in ^{40}Ca. The histogram gives B' (GT) values integrated over 250 keV intervals expressed in units of 1/MeV.

5. SUMMARY AND CONCLUSIONS

The total particle branching ratios in the $T_z = -1$, $A = 4n$ series are shown in table 17. If one assumes that the total β strength is roughly equal in these nuclides, then the particle branchings should increase when the available β-decay energy to particle emission increases. On the basis of quoted upper limits (see fig. 4) for the β-decay energy one can predict that the proton branchings should steadily increase as one goes from ^{20}Na to ^{40}Sc. The same is expected for the α-particle emission from ^{24}Al to ^{40}Sc but the rate of increase should be much slower. This is true for protons as can be seen from table 17 but for α particles it seems to fail. This may be due to the fact that the proton emission is so much more favourable in ^{36}K and ^{40}Sc that it corresponds to a major part of the β intensity.

The penetrabilities of the particle groups with the lowest energy vary on a very wide range from 10^{-2} to 10^{-7} and a general rule for the effective threshold cannot be given. The smallest penetrabilities for α particles are about an order of magnitude lower than those for protons. This reflects the common feature in these nuclei that the reduced α widths are about 1 % of the Wigner limit while for protons they are often below 0.1 %. Thus the states observed in this study are rather four-particle states than single-proton states.

In the lower sd shell β decay populates states which have reduced α widths comparable to the Wigner limit and therefore they are expected to be quite pure α-cluster states. The α clustering seems to decrease towards the upper part of the shell. This is in agreement with the general trend that with an increase in the level density in heavier nuclei there will occur stronger mixing of states. Because of this individual α-cluster properties vanish.

Table 17. Summary of delayed particle emission in the $T_z = -1$ series

precursor	I_p^{tot} $(\times 10^{-6})$	I_α^{tot} $(\times 10^{-6})$
^{20}Na	-	202000 ± 1900
^{24}Al	-	340 ± 90
^{24m}Al	-	280 ± 90
^{28}P	13 ± 4	9 ± 3
^{32}Cl	260 ± 50	540 ± 80
^{36}K	480 ± 140	35 ± 15
^{40}Sc	4400 ± 700	170 ± 50

The shell model seems to describe very well the β-decay transition rates in the sd shell, although there is evidence that in some cases the β-decay strength is split over two or more separate states. Some of the discrepancies between observation and shell-model predictions apparently arise from the omission of the $f_{7/2}$ orbit in the model space. However, these states are expected to be mainly populated by β decay through configuration mixing with sd-shell states. Although the assignment of the calculated levels to the experimentally observed ones is uncertain, a mutual compatibility can be obtained in log ft values in excitation energies. The difference in log ft values is in most cases less than 10 % and the difference in excitation energies less than 0.5 MeV. The mutual compatibility indicates that the main configuration consists of the sd shells despite the high excitation energy.

Delayed particle emission offers a sensitive means to study weak β branchings in the decay of a precursor nuclide. The weakest particle branchings observed in this work have been of the order of 10^{-7}. However, in many cases the γ emission competes with equal intensity with the particle emission and thus also other detection methods are needed. This is especially required near the threshold of particle emission.

The nuclear spectroscopic data derived from resonance reaction studies is valuable in the interpretation of the delayed particle spectra. However, delayed particle measurements can also bring new insight and complementary elements into the field of resonance studies. Such is the case, as shown in this work, when both protons and α particles are observed to be emitted from the same excited state in the emitter. Then the ratio of partial widths Γ_α/Γ_p is measured directly. In contrast, in resonance reaction studies this ratio is determined from two separate particle resonance experiments. Delayed particle studies can also serve as a useful guide for new resonance reaction studies in cases where hitherto unknown levels in the emitter are revealed in the observed particle spectra. It thus appears that a well coordinated effort to take advantage of the complementary aspects in the resonance reaction and delayed particle emission studies will be fruitful.

References

1) J.C. Hardy, in Nuclear Spectroscopy and Reactions, Part C, ed. J. Cerny (Academic Press, New York, 1974) pp. 417 - 466

2) J. Cerny and J.C. Hardy, Ann. Rev. Nucl. Sci. 27 (1977) 333

3) Proc. 3rd Int. Conf. on Nuclei far from Stability, Cargese, Corsica, 1976, CERN Rep. 76 - 13

4) Proc. 4th Int. Conf. on Nuclei far from Stability, Helsingør, 1981, CERN Rep. 81 - 09

5) D.F. Torgerson, K. Wien, Y. Fares, N.S. Oakey, R.D. Macfarlane and W.A. Lanford, Phys. Rev. C 8 (1973) 161

6) J.E. Steigerwalt, J.W. Sunier and J.R. Richardson, Nucl. Phys. A137 (1969) 585

7) D.F. Torgerson, N.S. Oakey and R.D. Macfarlane, Nucl. Phys. A178 (1971) 69

8) R.I. Verrall and R.E. Bell, Nucl. Phys. A127 (1969) 635

9) R.G. Sextro, R.A. Gough and J. Cerny, Phys. Rev. C 8 (1973) 258

10) G.T. Ewan, E. Hagberg, J.C. Hardy, B. Jonson, S. Mattsson and P. Tidemand-Petersson, Nucl. Phys. A337 (1980) 189

11) B.A. Brown and B.H. Wildenthal, shell-model calculations in sd shell, private communication and to be published

12) S. Raman, C.A. Houser, T.A. Walkiewicz and I.S. Towner, Atomic Data and Nuclear Data Tables 21 (1978) 567

13) A. Bohr and B.R. Mottelson, in Nucl. Structure, (Benjamin Inc., New York, 1969), vol. I, p. 345

14) B.J. Brussaard and P.W.M. Glaudemans, in Shell-Model Applications in Nuclear Spectroscopy (North-Holland, Amsterdam, 1977) p. 263

15) J.B. McGrory and B.H. Wildenthal, Ann. Rev. Nucl. Part. Sci 30 (1980) 383

16) I.S. Towner, J.C. Hardy and M. Harvey, Nucl. Phys. A284 (1977) 269

17) D.H. Wilkinson, Phys. Lett. 67B (1977) 13

18) I.S. Towner and J.C. Hardy, Phys. Lett. 73B (1978) 20

19) N.B. Gove and M.J. Martin, Nucl. Data Tables 10 (1971) 205

20) S. Raman and N.B. Gove, Phys. Rev. C 7 (1973) 1995

21) J.D. Anderson, C. Wong and J.W. McClure, Phys. Rev. 138B (1965) 615

22) A. Arima, H. Horiuchi, K. Kubodera and N. Takigawa, Advances in Nuclear Physics 5 (1972) 345 - 477

23) J.B. Marion and F.C. Young, in Nuclear Reaction Analysis: Graphs and Tables (North-Holland, Amsterdam, 1968) p. 327

24) J. Äystö, thesis, University of Jyväskylä, Department of Physics, 1977, unpublished

25) S.E. Vandenbosch, C.V.K. Baba, P.R. Christensen, O.B. Nielsen and H. Nordby, Nucl. Phys. 41 (1963) 482

26) P.D. Ingalls, Phys. Rev. C 14 (1976) 254

27) J. Honkanen, M. Kortelahti, J. Äystö, K. Eskola and A. Hautojärvi, Physica Scripta 19 (1979) 239

28) E.K. Warburton, C.J. Lister, D.E. Alburger and J.W. Olness, Phys. Rev. C 23 (1981) 1242

29) C. Détraz, Nucl. Phys. A188 (1972) 513

30) C. Détraz, C.S. Zaidins, D.J. Frantsvog, R.L. Wilson and A.R. Kunselman, Nucl. Phys. A203 (1973) 414

31) D.W. Miller, F. Everling, D.A. Outlaw, T.G. Dzubay, A.A. Jaffe, G.A. Bissinger and S.M. Shafroth, Phys. Rev. C 6 (1972) 869

32) F. Ajzenberg-Selove, Nucl. Phys. A300 (1978) 1

33) B.A. Brown, W. Chung and B.H. Wildenthal, Phys. Rev. Lett. 40 (1978) 1631

34) H.T. Fortune, R.R. Betts and R. Middleton, Phys. Lett. 62B (1976) 287

35) H.T. Fortune, R. Middleton and R.R. Betts, Phys. Rev. Lett. 29 (1972) 738

36) R.D. Macfarlane, N.S. Oakey and R.J. Nickles, Phys. Lett. 34B (1971) 133

37) E.T.H. Clifford, J.C. Hardy, H. Schmeing, R.E. Azuma, H.C. Evans, T. Faestermann, E. Hagberg, K.P. Jackson, V.T. Koslowsky and U.J. Schrewe, Proc. 4th Int. Conf. on Nuclei far from Stability, Helsingør, 1981, CERN Rep. 81 - 09, p. 306

38) T. Tomoda and A. Arima, Nucl Phys. A303 (1978) 217

39) P.M. Endt and C. van der Leun, Nucl. Phys. A310 (1978) 1

40) D. Kelvin, A. Watt and R.R. Whitehead, J. of Phys. G 3 (1977) 1539

41) T.-A. Shibata, J. Imazato, T. Yamazaki and B.A. Brown, J. Phys. Soc. of Japan 47 (1979) 33

42) L.K. Fifield, M.J. Hurst, T.J.M. Symons, F. Watt, C.H. Zimmerman and K.W. Allen, Nucl. Phys. A309 (1978) 77

43) L.K. Fifield, E.F. Garman, M.J. Hurst, T.J.M. Symons, F. Watt, C.H. Zimmerman and K.V. Allen, Nucl. Phys. A322 (1979) 1

44) A. Gobbi, P.R. Maurenzig, L. Chua, R. Hadsell, P.D. Parker, M.W. Sachs, D. Shapira, R. Stokstad, R. Wieland and D.A. Bromley, Phys. Rev. Lett. 26 (1971) 396

45) J. Honkanen, M. Kortelahti, K. Valli, K. Eskola, A. Hautojärvi and K. Vierinen, Nucl. Phys. A330 (1979) 429

46) P.M. Endt, private communication

47) J.W. Maas, E. Somorjai, H.D. Graber, C.A. van den Wijngaart, C. van der Leun and P.M. Endt, Nucl. Phys. A301 (1978) 213

48) M.A. Meyer, I. Venter and D. Reitmann, Nucl. Phys. A250 (1975) 235

49) B.M. Paine, S.R. Kennett and D.G. Sargood, Phys. Rev. C 17 (1978) 1550; B.M. Paine and D.G. Sargood, Nucl. Phys. A331 (1979) 389

50) A. Tveter, Nucl. Phys. A185 (1972) 433

51) H. Nakayama, M. Ishii, K. Hisatake, F. Fujimoto and K. Komaki, Nucl. Phys. A208 (1973) 545

52) E. Fuschini, F. Malaguti, A. Uguzzoni and E. Verondini, Phys. Rev. C 21 (1980) 1646

53) R.B. Alexander, J.U. Andersen and K.G. Prasad, Nucl. Phys. A279 (1977) 278

54) F. Malaguti, A. Uguzzoni and E. Verondini, Phys. Rev. C 19 (1979) 1606

55) D.W.O. Rogers, W.R. Dixon and R.S. Storey, Nucl. Phys. A281 (1977) 345

56) W.F. Coetzee, M.A. Meyer and D. Reitmann, Nucl. Phys. A185 (1972) 644

57) R. O'Brien, Z.E. Switkowski, A.K. Smith and D.G. Sargood, Aust. J. Phys. 28 (1975) 155

58) J. Vernotte, S. Gales, M. Langevin and J.M. Maison, Nucl. Phys. A212 (1973) 493

59) K. Eskola, M. Riihonen, K. Vierinen, J. Honkanen, M. Kortelahti and K. Valli, Nucl. Phys. A341 (1980) 365

60) L.C. Northcliffe and R.F. Schilling, Nucl. Data Tables A7 (1970) 233

61) P.M. Johnson, M.A. Meyer and D. Reitmann, Nucl. Phys. A218 (1974) 333

62) G.A. Hokken, J.A.J. Hermans and A. van Ginkel, Nucl. Phys. A211 (1973) 405

63) B. Bosnjakovic, J. Bouwmeester, J.A. van Best and H.S. Pruys, Nucl. Phys. A110 (1967) 17

64) F.C. Erne, Nucl. Phys. 84 (1966) 241

65) J.C. Hardy, H. Brunnader and J. Cerny, Phys. Rev. Lett. 22 (1969) 1439

66) M.J. Fritts, Phys. Rev. C 13 (1976) 331

67) J. Honkanen, M. Kortelahti, K. Valli, J. Äystö, K. Eskola, A. Hautojärvi and K. Vierinen, JYFL Annual Report 1978, 3.3., and to be published

68) R.J. de Meijer, A.A. Sieders, H.A.A. Landman and G. De Roos, Nucl. Phys. A155 (1970) 109

69) T. Nakashima, J. Phys. Soc. of Japan 36 (1974) 10

70) R. van der Borg, M.N. Harakeh and A. van der Woude, Nucl. Phys. A365 (1981) 243

71) H.P. Leenhouts and P.M. Endt, Physica 32 (1966) 322

72) P.M. Endt, Atomic Data and Nucl. Data Tables 23 (1979) 3

73) Shang Ren-Cheng, A.A. Pilt, J.A. Kuehner, M.A.M. Shahabuddin and A. Trudel, Nucl. Phys. A366 (1981) 13

74) H.P. Leenhouts, Physica 35 (1967) 290

75) V. Gillet and E.A. Sanderson, Nucl. Phys. A91 (1967) 292

76) W.J. Gerace and A.M. Green, Nucl. Phys. A113 (1968) 641

77) A.M. Green, private communication